SWITCHING THE REFLECTION IN CHIRAL NEMATIC MESOPOROUS SILICA AND ORGANOSILICA FILMS

by

Joanna Christine De Witt

B.Sc., McGill University, 2010

A THESIS SUBMITTED IN PARTIAL FULFILLMENT OF THE REQUIREMENTS FOR THE DEGREE OF

MASTER OF SCIENCE

in

The Faculty of Graduate Studies

(Chemistry)

THE UNIVERSITY OF BRITISH COLUMBIA

(Vancouver)

December 2012

Abstract

Recently, a new class of free-standing chiral nematic mesoporous silica and organosilica films was developed using nanocrystalline cellulose as a template. Due to their unique structures these films are iridescent, and by varying synthetic conditions it has been shown that this iridescence can be tuned to selectively reflect incident light of different wavelengths across the entire visible spectrum. However, upon formation of the mesostructure, these optical properties are locked in and can no longer be altered. Herein I describe alternate techniques to modify the optical properties of these silica and organosilica films by infiltration with guest molecules after the films have been prepared.

Liquid crystal mesogen 5CB and 8CB were loaded into the pores of unfunctionalized and octyl and phenyl functionalized silica films. Thermal cycling of these new composite materials elucidated a sharp and reversible optical change in the 8CB loaded octyl functionalized silica films. Additional studies including variable temperature POM and UV-Vis spectroscopy were conducted on this system prepared with organosilica films. This approach was then expanded on by doping an azobenzene derivative in 1, 5, and 10 % by weight into the 8CB liquid crystal before loading the mixtures into the films. A reversible optical change was then brought about in this system by irradiation at different wavelengths. Further development of these methods could lead to their implementation in the still emerging fields of sensing and display technologies involving colour information.

Preface

Prof. Mark MacLachlan was the supervisor for all of the chapters presented in this thesis. Dr. Wadood Hamad from FPInnovations, Vancouver, BC, Canada was a collaborator throughout and supplied us with the nanocrystalline cellulose used to carry out the work. Kevin Shopsowitz acted as a colleague and collaborator for all of the work.

Portions of Chapters 1 and 2 have been prepared for publication as: De Witt, J. C., Shopsowitz, K. E., Hamad, W. Y., MacLachlan, M. J. "Thermal Switching of the Reflection in Chiral Nematic Mesoporous Organosilica Films Infiltrated with Liquid Crystals" *in prep.* I was the principle author of this work and co-edited it with Prof. Mark MacLachlan, Kevin Shopsowitz, and Dr. Wadood Hamad. I carried out all of the experiments conducted in Chapter 2 with the exception of the synthesis of the mesoporous silica and organosilica films, the procedure for which was first developed by Kevin Shopsowitz, but then repeated and slightly modified by me.

I collaborated with Kevin Shopsowitz for portions of Chapter 3. He synthesized and characterized the azobenzene dopant precursor, diazene, 1-(4-butylphenyl)-2-(4-hydroxyphenyl). I performed all of the other experiments conducted in the chapter.

Table of Contents

List of Figures

List of Schemes

List of Symbols

@	encapsulated in
n	refractive index
n_{avg}	average refractive index
P	pitch
Δn	birefringence
λ	wavelength
λ_{max}	wavelength of maximum intensity

List of Abbreviations

5CB	4-cyano-4’-pentylbiphenyl
8CB	4-cyano-4’-octylbiphenyl
AB	azobenzene
ABD	azobenzene dopant
ASAP	Accelerated Surface Area and Porosity
ATR	attenuated total reflectance
BET	Brunauer-Emmett-Teller
BJH	Barrett-Joyner-Halenda
BTMSE	1,2-bis(trimethoxysilyl)ethane
CN	chiral nematic
CN-LC	chiral nematic liquid crystal
CNMO	chiral nematic mesoporous organosilica
CNMS	chiral nematic mesoporous silica
DCM	dichloromethane
EISA	evaporation induced self-assembly
FT-IR	Fourier transform infrared
GLAD	glancing angle deposition
IR	infrared
IUPAC	International Union of Pure and Applied Chemistry

LC	liquid crystal
LCD	liquid crystal display
NCC	nanocrystalline cellulose
NIR	near infrared
NMR	nuclear magnetic resonance
POM	polarized optical microscopy
TEOS	tetraethyl orthosilicate
TGA	thermal gravimetric analysis
TMOS	tetramethyl orthosilicate
UV-Vis	ultraviolet-visible
XRD	X-ray diffraction

Acknowledgements

I would like to thank my supervisor, Prof. Mark MacLachlan, for his guidance and enthusiasm on this project. Mark's passion for his research is truly an inspiration. I would also like to thank Dr. Wadood Hamad for the NCC as well as for his invaluable advice. To the MacLachlan group members, past and present, thank you for your input, support, and friendship. I would especially like to thank Kevin Shopsowitz for getting me started on the project and for his help throughout. And to all the amazing friends I have made during my time at UBC, thanks for everything.

Lastly, I would like to thank my family for their unconditional love and support. To my parents and sisters – I would not be who I am or where I am today without you; to my family in Burnaby – it has been such a pleasure to have you so close; and especially to Oma – the love you put into your meals is unmatched, you have kept me and my friends more than well fed throughout these years. I love you all. I would also especially like to thank Opa without whom I may never have "come here" in the first place to spend two wonderful years in Vancouver. Rest in peace.

Chapter 1: Introduction

1.1 Chemistry of Light and Colour

The world all around us appears coloured. These colours are the result of light interacting with an object and being absorbed, transmitted, or reflected. If the wavelengths are within the range of visible light, those which the human eye can detect, then one or a combination of these effects allow us to see colours. Regardless of whether or not we can see their effects, these processes can occur with all wavelengths of light throughout the whole spectrum, and can be detected by other means. There are two general factors that determine which light is absorbed, transmitted, or reflected: chemical and physical properties. For example, dyes and pigments rely on the chemical properties of the molecules involved to produce colour through absorption of specific wavelengths of light.[1] Azobenzene derivatives can range from yellow to orange to red depending on their particular substitutions which give rise to subtle differences in their electronic absorption spectra.[2] However, colour can also be dictated based on the physical properties of an object and their effect on light. In fact there are many examples of periodic nanostructures which give rise to colouration due to interference, diffraction, or scattering of light from the physical structure of materials.[3,4,5] For example, in nature the periodic chitin nanostructures of many insects cause Bragg reflection of light which is responsible for their beautiful iridescent colours.[6] These types of structures can be purely organic, inorganic, or composite materials, and their interaction with light can yield a range of different colours. An advantage of colour generated by physical means is that it is generally more stable. As opposed to colour generated

by light absorption, the materials responsible for physical colouring do not have to absorb light which can excite molecules and change their reactivity and thus their stability. Furthermore, it is necessary to use a different molecule or compound to produce different colours from a material with colour originating from absorption, whereas more than a single physical colour can be produced from one material.[7]

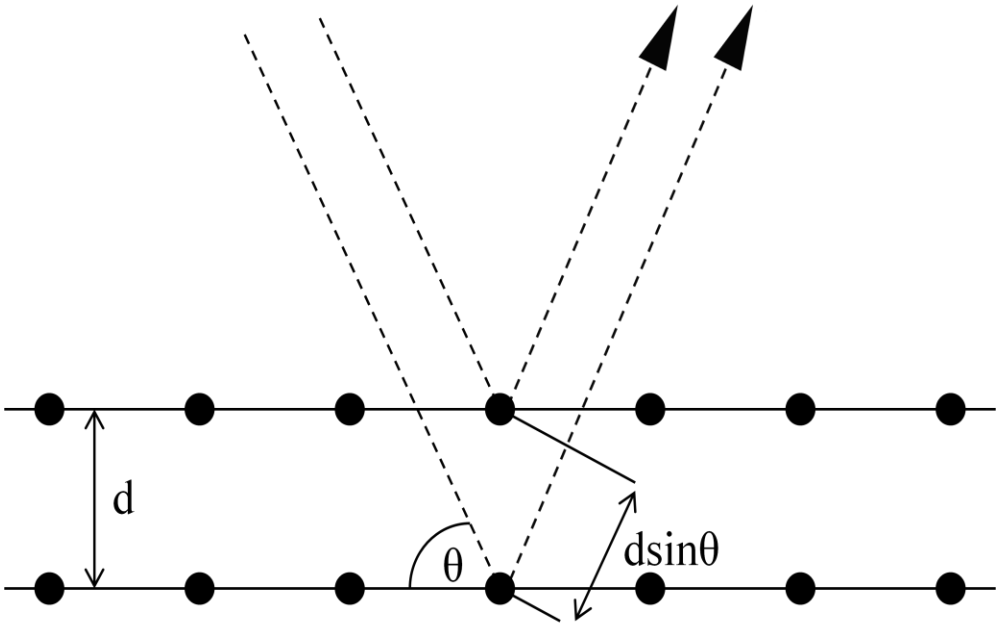

Figure 1-1. Graphical representation of Bragg diffraction where d is the distance between repeating features and θ is the angle of incident light. Adapted from reference 8.

Photonic crystals are materials patterned with periodically varying refractive indices that create a range of frequencies called the photonic bandgap, which forbids propagation of that certain frequency range of light. Photons with energies lying in the bandgap cannot propagate through the medium. The size and position of the bandgap depends on factors such as the repeating distance, refractive index contrast, and the specific ordering of the photonic crystal. If incident light falls within the photonic bandgap it is selectively reflected due to Bragg diffraction

(Figure 1-1), whereas if it falls outside of the photonic bandgap it is transmitted.[9] This behaviour can give rise to interesting optical properties. For instance, photonic crystals can appear coloured if their features are on the length scale of visible light. They occur naturally in many forms, but they can also be manmade. Photonic crystals can be classified as one-dimensional, two-dimensional, or three-dimensional depending on their organization (Figure 1-2).[10] A Bragg grating, which consists of alternating layers of materials with different refractive indices with characteristic repeating distance, is an example of a one-dimensional photonic crystal. An example of a two-dimensional photonic crystal is a substrate with periodically drilled holes designed to be transparent to the wavelength of radiation that the bandgap is to block. Examples of three-dimensional photonic crystals include opals and inverse opals (Figure 1-3).[11] Due to their interesting properties, photonic crystals have found use in a wide range of applications. One of their first commercial uses was found in fibre optics and waveguides. Porous photonic crystals also have shown potential in sensing due to the ability for guests to bring about a colour change by varying the refractive index contrast within the material.[12,13]

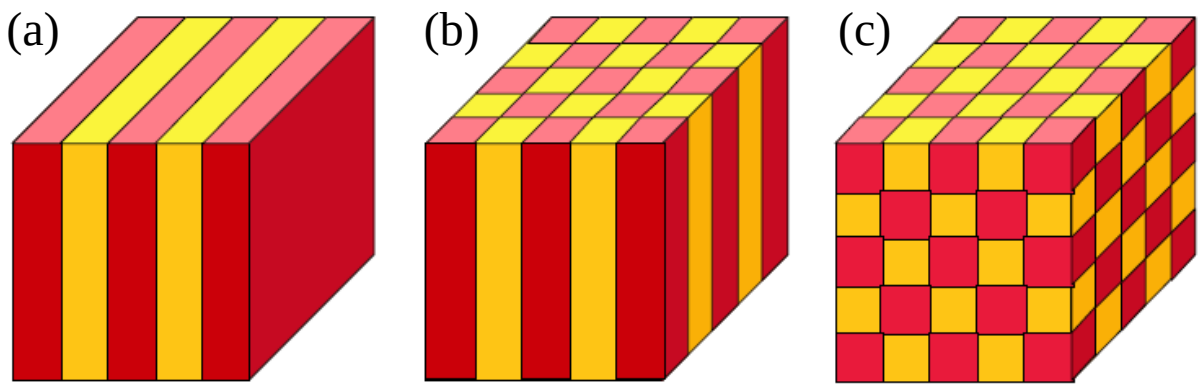

Figure 1-2. Representations of (a) 1D (b) 2D and (c) 3D photonic crystals.

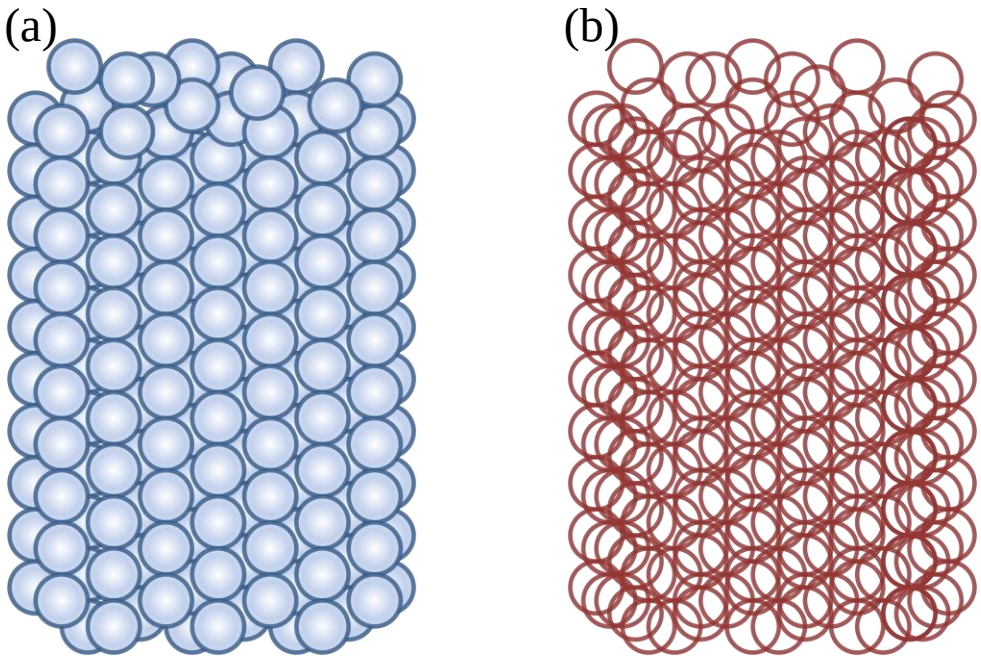

Figure 1-3. Schematic of (a) an opal and (b) and inverse opal. Adapted from reference 11.

1.2 Liquid Crystals

Liquid crystals (LCs) have properties intermediate to those of solids and liquids. They flow like a liquid, but also have the crystal-like orientational and/or positional ordering of a solid.[14] There are two general types of liquid crystals: thermotropic and lyotropic. Thermotropic phases occur within a certain temperature range above which the sample is isotropic and below which it is crystalline. Lyotropic liquid crystals exhibit phase transitions as a function of the concentration of LC molecules in a solvent, but they can also be influenced by temperature or other factors. Liquid crystalline phases are characterized by their degree and type of ordering, which can be short-range or long-range positional and/or orientational order. These phases rely on self-assembly of the LC molecules involved which is governed by their fundamental order-inducing units or mesogens. One of the most common LC phases is the nematic phase, which consists of rod-shaped molecules with long-range directional order, but no positional order. Smectic liquid crystal phases are found at lower temperatures than the nematic and have an additional positional order along one direction to form layers.

The chiral nematic phase, or cholesteric phase (so named because it was first observed by Reinitzer in cholesterol derivatives),[15] exhibits a twisting of adjacent molecules parallel to the nematic director due to their asymmetric packing and results in long-range chiral order. Chiral nematic phases can be observed for thermotropic or lyotropic LCs, and can form either due to the chirality of the molecules themselves or through the addition of a chiral dopant. Chiral nematic liquid crystals (CN-LCs) have a characteristic pitch, which refers to the distance over which the director makes a full 360° twist. If this pitch is on the order of the wavelength of visible light,

CN-LCs appear coloured. This is because they behave as one-dimensional photonic crystals, since the helical ordering of the nematic director leads to a periodically changing refractive index within the material. The selective reflection of light from a CN-LC occurs according to the following equation:

$$\lambda = P \cdot n_{avg} \cdot \sin\theta \qquad (1)$$

in which the wavelength of light reflected (λ) is related to the helical pitch (P), the average refractive index (n_{avg}), and the angle of incidence (θ).[16] In equation 1, λ corresponds to the center of the reflection peak, while the width is given by the following equation:

$$\Delta\lambda = P\Delta n \qquad (2)$$

where Δn corresponds to the birefringence of the liquid crystal. Additionally, reflection from a CN-LC only occurs for light with a circular polarization that matches the handedness of the helical structure (Figure 1-4). Only right-handed circularly polarized light will be reflected from a right-handed chiral nematic structure, and only left-handed circularly polarized light will be reflected from a left-handed chiral nematic structure, and for both cases the handedness of the polarization does not flip upon reflection.

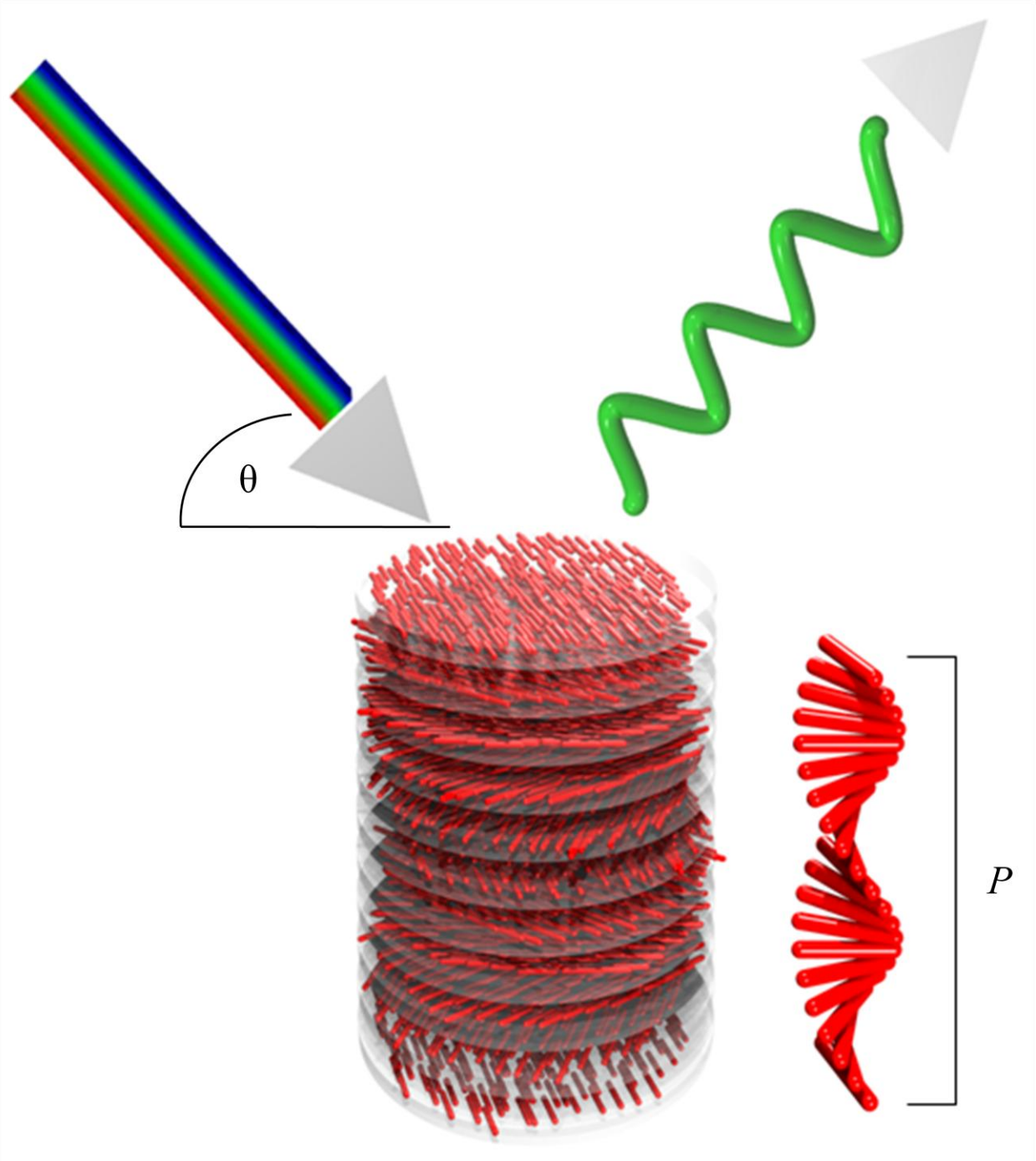

Figure 1-4. Schematic representation of diffraction from a CN-LC. Adapted from reference 41.

1.3 Nanocrystalline Cellulose

Cellulose is a linear polysaccharide with the formula $(C_6H_{10}O_5)_n$ consisting of a chain of hundreds to thousands of β-1,4 linked D-glucose units (Figure 1-5). Cellulose is the primary structural component in plants and trees and is the most common organic compound on earth, making it one of the most abundant and renewable resources available.[17] Its fibres are widely used industrially in the pulp and paper industry and in textiles, mainly obtained from wood pulp and cotton. Cellulose has remarkable mechanical properties and stability.[18] The straight chain polymer adopts a rather stiff rod-like conformation and neighbouring chains form hydrogen bonds (Figure 1-6) holding them firmly together and imparting high tensile strength on the microfibrils they form.[19,20] Cellulose is insoluble in water and most organic solvents, however cellulose can be functionalized to form soluble derivatives.

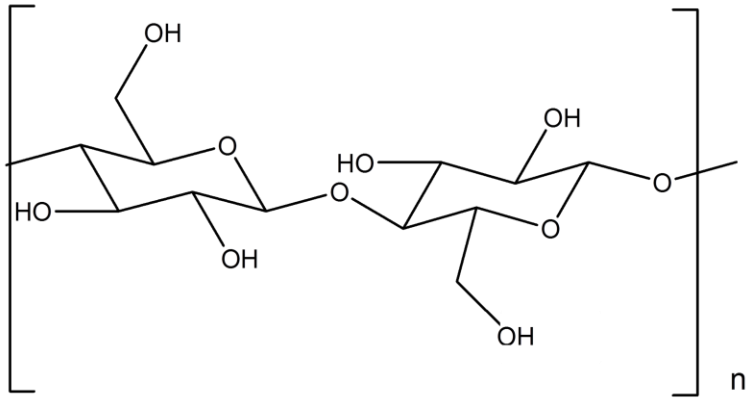

Figure 1-5. Chemical structure of cellulose.

Cellulose fibres used in industrial applications are typically tens of micrometers in width with lengths ranging from several millimeters to centimeters. These fibres can be broken down

further using chemical approaches to obtain nanoscale cellulose materials. Nanocrystalline cellulose (NCC) consists of rigid, rod-like particles produced by the acid hydrolysis of cellulose (Figure 1-7). The amorphous regions of cellulose are more susceptible to acid catalyzed hydrolysis than the highly crystalline regions, so they can be selectively removed under the right conditions to isolate the NCC particles which are typically purified by centrifugation and dialysis.[21,22] When derived from plant sources NCC particles have diameters of ~3-20 nm and lengths of ~100-300 nm; the exact dimensions depend largely on the specific cellulose source and exact method of preparation.

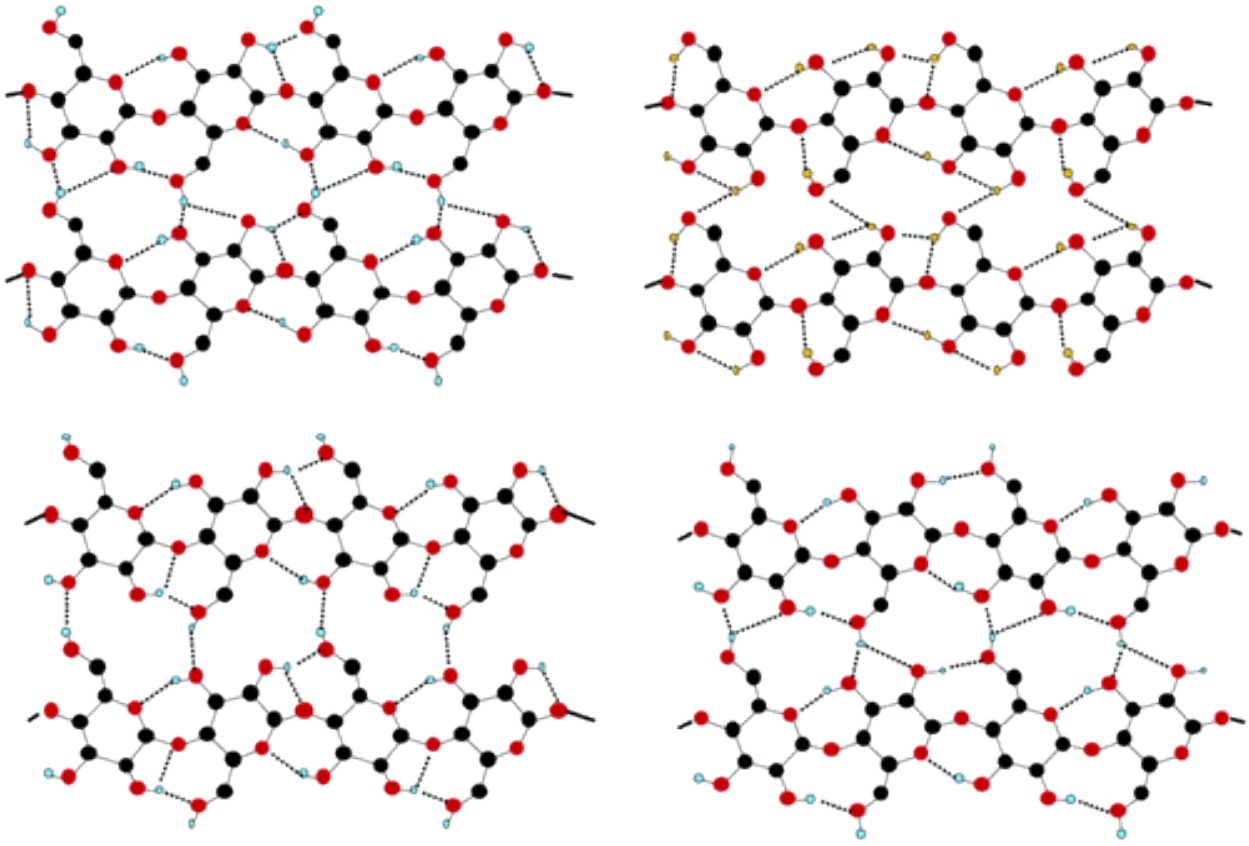

Figure 1-6. Some possible hydrogen bonding structures of cellulose. Reproduced in part with permission from reference 20. Copyright 2004 American Chemical Society.

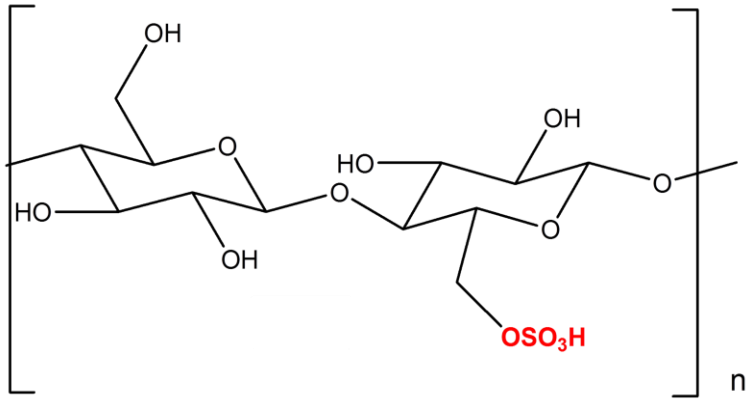

Figure 1-7. Modified chemical structure of cellulose after sulfuric acid hydrolysis.

Nanocrystalline cellulose suspensions exhibit a chiral nematic phase. This was first reported by Revol et al. in 1992.[23] Above the critical concentration of NCC, a chiral nematic phase spontaneously separates out. This phase is in equilibrium with the isotropic phase, which will disappear at high concentrations of NCC. On drying by slow evaporation, this phase can solidify into twisted layers that retain the chiral nematic organization. The helical pitch of NCC suspensions is typically on the order of microns, however a significant decrease occurs upon drying due to the increase in concentration that occurs with evaporation. The resultant films exhibit selective reflection of light and can appear coloured if that reflection falls within the wavelengths of the visible region. Factors such as temperature, ions present, aspect ratio, external field, and preparation conditions can influence the chiral nematic self-assembly of NCC.[24,25,26,27,28] By varying one or many of these factors, the pitch can be tuned to alter the properties of the resultant NCC films and produce films of different colours. It should also be noted that due to the inherent chirality of the cellulose source, only left-handed structures (suspensions and films) have been observed for NCC.

There are many potential applications for NCC due to its mechanical properties (strength and high surface area), hydrophilicity, dispersibility and functionalization potential, and non-toxicity and environmentally friendly nature.[29,30] For example NCC has found use as a filler additive in polymer materials.[31]

1.4 NCC as a Template

Templation is a common chemical practice which involves the use of molecules or larger particles or objects to serve as a pattern for the synthesis of a consistent product. The template is the structure which imparts order on the other species, and then after that design is transferred, is removed. For example the use of a photolithographically patterned surface to transfer a design or more generally the use of an inflated balloon for producing shaped papier maché are examples of templation. Supramolecular chemistry can also involve templates in template-directed synthesis, which involves the self-assembly of molecules through non-covalent interactions to pre-organize the system for a chemical reaction. For example, the combination of a surfactant liquid crystal with an inorganic precursor followed by condensation and template removal results in a porous inorganic solid.[32]

Templation is often used in order to prepare porous materials, which can be either microporous (<2 nm), mesoporous (2-50 nm), or macroporous (>50 nm) as defined by IUPAC. [33] The intermediate size regime of mesopores can be especially advantageous as the pores are large enough to be infiltrated by various guests, but small enough to give high specific surface areas. Mesoporous silica was the first ordered mesoporous material to be prepared by template synthesis.[34,35] Typically, mesoporous silica is synthesized under aqueous conditions with a tetraalkoxysilane silica precursor, such as tetramethyl orthosilicate (TMOS) or tetraethyl orthosilicate (TEOS). A solid silica network is formed by hydrolysis and condensation reactions around the template, which can then be removed through calcination or solvent extraction to give mesoporous silica. Mesoporous organosilicas have also been synthesized in a similar manner,

but using bridged precursors of the general type $(R'_3O)_3Si\text{-}R\text{-}Si(OR'_3)_3$.[36,37,38] This sol-gel chemistry is very versatile and generally quite robust and can be carried out over a wide range of conditions resulting in mesoporous silicas and organosilicas with many different structures and morphologies.

Nanocrystalline cellulose has the perfect dimensions to serve as a template to form mesoporous materials. Furthermore its properties are advantageous in a sol-gel approach. In 2003, Mann *et al.* reported the use of NCC as a template to form mesoporous silica.[39] Unfortunately, while the size dimensions of NCC were transferred to the pores of the resultant materials, the chiral nematic organization was lost.

Although this early attempt to transfer the chiral nematic organization of an NCC template to the resultant silica material was unsuccessful, more recently our group was able to do just that by controlling the pH and concentration of the aqueous NCC suspension prior to its use as a templation agent.[40] It was found that a 3 weight % suspension of NCC at pH = 2.4 retained its chiral nematic phase upon evaporation induced self-assembly (EISA) in the presence of a silica precursor, thus imparting that order onto the silica, which remained in the pores even after NCC removal. Additionally, the helical pitch of the pores in the resultant chiral nematic mesoporous silica films could be tuned by varying the concentrations of the precursors to be on the order of the wavelength of light throughout the visible spectrum and into the infra red, such that the films appeared coloured due to the selective reflection of those wavelengths (Figure 1-8). This was also recently accomplished using an organosilica precursor resulting in chiral nematic mesoporous organosilica films with improved flexibility over the brittle silica films and similar optical properties.[41] It was also shown that by infiltrating these films with isotropic liquids of a near refractive index match that the selective reflection could essentially be shut off, but upon

drying they revert back to their coloured, iridescent form (Figure 1-9). These new materials show promise in chiral separations, sensing, and decorative applications.

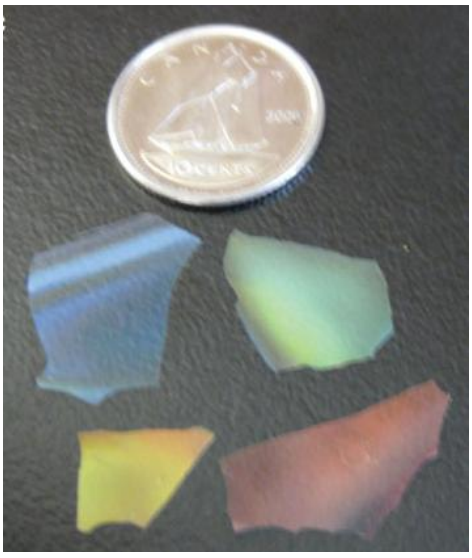

Figure 1-8. Photograph showing the range of colours attainable in the silica films. Reproduced in part with permission from reference 40. Copyright 2010 Nature Publishing Group.

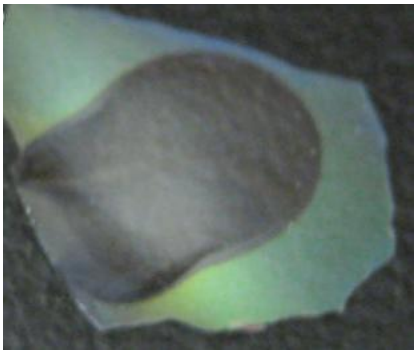

Figure 1-9. Photograph of a silica film depicting the significant optical change after addition of a drop of water.

1.5 Overview of the Thesis

The goal of this thesis is to develop new methods to modify and tune the optical properties of free-standings films of chiral nematic mesoporous silica and organosilica. Once the films are formed their properties are locked in place, however by the incorporation of guests it is possible to alter these after the fact by other means. Furthermore, by the incorporation of responsive guests with stimuli induced optical changes themselves, it is possible to induce additional multiple optical changes after the guests have been incorporated into the pores. These new composite materials should hold potential for use in real world applications such as for sensors and displays.

In Chapter 2, I present four new silica-LC composite materials, which exhibit thermally induced, fully reversible optical changes. Based on their behaviour, I then present an additional composite material, organosilica-LC, with enhanced properties, which also exhibits the desired thermally induced, fully reversible optical change. I report the preparation, characterization, and variable temperature studies for all of these materials. Additionally, I attempt to explain and interpret the results of this work.

In Chapter 3, I introduce an additional set of organosilica-LC composite materials, this time including an azobenzene component doped into the LC in various proportions. These materials exhibit irradiation-induced reversible optical changes. I then report the preparation and characterization of the azobenzene dopant, as well as the preparation, characterization, and irradiation studies for all of these composite materials. Additionally, I again attempt to explain and interpret the results of this work.

Finally, in Chapter 4, I come to some general conclusions and put forward some ideas for future directions of this work.

Chapter 2: Liquid Crystal Loading

2.1 Introduction

Many sensors and display technologies, such as temperature sensors and liquid crystal displays (LCDs), depend on controlling the order in liquid crystalline materials.[42,43,44,45] Chiral nematic liquid crystals (CN-LCs) are an important family of liquid crystals that have a helical organization of mesogens.[15] The repeating distance, or pitch, of a CN-LC can be modified by changing the temperature or pressure, or by applying an external field.[46,47,48,49,50] One intriguing property of CN-LCs is that they selectively reflect wavelengths of light that depend on the pitch of the chiral nematic phase.[51] The reflected light is circularly polarized, and its handedness matches the helicity of the chiral nematic structure.[52,53,54] CN-LCs are thus useful for developing sensors and displays.[55]

The selective reflection of light, as observed for CN-LCs, is a fundamental property of photonic crystals. Photonic crystals, which are structures with a periodically varying refractive index, are another class of materials that are attractive for developing advanced technologies.[9,12,56,57,58] By modulating the refractive index of substances located within the pores of a photonic crystal, one may modify the optical properties of the structures and control the wavelengths of light that are transmitted. Photonic crystals infiltrated with liquid crystals are being used to develop new tunable photonic structures where the optical properties (e.g., position of the stop band) can be modulated by changes in temperature or other external stimuli.[59,60] For example, a

photonic crystal infiltrated with 4-cyano-4'-pentylbiphenyl (5CB) showed polarization-dependent optical properties that depend on the orientation of the liquid crystal in the nematic phase.[61] In another study, indium phosphide-based planar photonic crystals were infiltrated with a nematic liquid crystal and also showed optical properties that depend on the orientation of the liquid crystal.[62] Other examples of photonic structures infiltrated with liquid crystals are known.[63,64,65]

Brett and co-workers have used glancing-angle deposition (GLAD) to fabricate porous, chiral thin films with optically anisotropic helical microstructures.[66,67,68,69,70,71] Their porous thin films offer an alternative approach to LC alignment that provides a greater level of control than alignment by substrate surface treatments alone. The porous thin film can act as a host and provide a large surface area contact for embedded guest LCs, allowing for long-range orientation control over the entire thickness of the film. Through the use of this novel method, they obtained LC infiltrated films with enhanced optical properties, including reduced scattering and increased birefringence compared to the unloaded GLAD films. Additionally, the switching of LCs in a GLAD film under the influence of an applied field was explored, and preliminary results indicated that switching remains possible and can lead to a significant change in circular dichroism.[72,73, 74,75]

Our group recently reported convenient methods to make free-standing mesoporous silica,[40] organosilica,[41] or carbon films[76] with tunable chiral nematic pore structures. This was accomplished through sol-gel synthesis in the presence of nanocrystalline cellulose (NCC), which serves as a chiral nematic template. NCC is extracted as a colloidal suspension by acid hydrolysis of cellulosic materials, typically bleached chemical wood pulps, but other sources, such as bacteria or cotton can also be used.[77,78,79,80] After combustion of the NCC, the resulting

silica films are mesoporous and have a chiral nematic organization of pores. Consequently, the films show selective reflection of light that can be tuned from the near-IR to the UV. By using the organosilica precursor bis(trimethoxysilyl)ethane (BTMSE), we are able to create mesoporous organosilicas that are less brittle than the pure silica analogues, but retain the same chiral nematic pore structure and optical properties.

In this chapter, I set out to modify the reflectivity of the silica and organosilica films by infiltrating the mesopores with a stimulus-responsive guest. 4-Cyano-4'-pentylbiphenyl (5CB) and 4-cyano-4'-octylbiphenyl (8CB), thermotropic liquid crystals (Figure 2-1),[81] were identified as excellent candidates since they are commercially available and their thermal properties have been extensively studied. In the following, I describe the synthesis of phenyl functionalized and

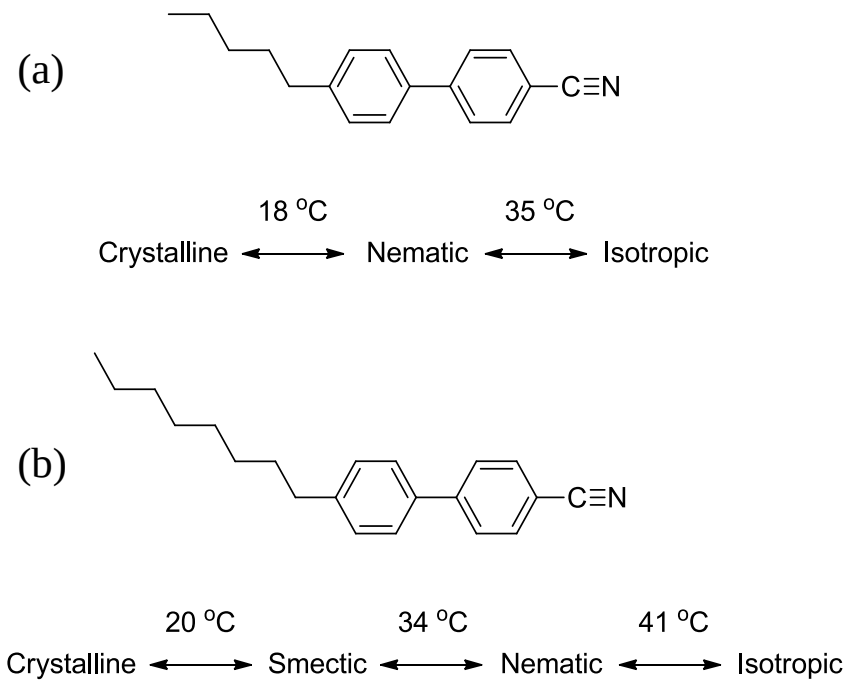

Figure 2-1. Structures and transition temperatures of thermotropic liquid crystals (a) 5CB and (b) 8CB.

octyl functionalized mesoporous silica and octyl functionalized mesoporous organosilica, their infiltration with LC guests, and subsequent investigations of these new composite materials' reversibly switchable optical properties. The composites are iridescent, show a peak reflected wavelength in the visible range, and undergo a sharp, reversible transition around 35 °C or 40 °C (depending on which LC is involved), above which colourless, transparent films are obtained. This unique switching of a guest within the pores of the chiral nematic solid-state host may serve as the basis of a tunable filter or display.

2.2 Experimental

Materials.

NCC was obtained as a suspension in water (pH 2.4). 1,2-Bis(trimethoxysilyl)ethane, 1-(triethoxysilyl)octane, and phenyltrimethoxysilane were obtained from Sigma Aldrich; all were used without further purification. 5CB and 8CB were obtained from Synthon Chemicals. Hydrochloric acid (36.5 - 38%), sulfuric acid (95 - 98%), and hydrogen peroxide (30 - 31.6%) were used as received from Fisher Scientific or further diluted where specified. Toluene was dried over activated alumina prior to use.

Preparation of nanocrystalline cellulose.

For the preparation of nanocrystalline cellulose (NCC) fully-bleached, commercial kraft softwood pulp was first milled to pass through a 0.5-mm screen in a Wiley mill to ensure particle size uniformity and to increase surface area. The milled pulp was hydrolysed in sulfuric acid (8.75 ml of a sulfuric acid solution per gram of pulp) at a concentration of 64 wt% and a temperature of 45 °C with vigorous stirring for 25 min. The cellulose suspension was then diluted with cold de-ionized water (about ten times the volume of the acid solution used) to stop the hydrolysis, and allowed to settle overnight. The clear top layer was decanted and the remaining cloudy layer was centrifuged. The supernatant was decanted and the resulting thick white suspension was washed three times with de-ionized water to remove all soluble cellulose materials. The thick white suspension obtained after the last centrifugation step was placed inside

dialysis membrane tubes (12,000–14,000 molecular weight cut-off) and dialysed against slow running de-ionized water, for 1 to 4 days. The membrane tubes containing the extracted cellulose materials were placed periodically in de-ionized H_2O, and the procedure was continued until the pH of the water became constant for a period of one hour. The suspension from the membrane tubes was dispersed by subjecting it to ultrasound treatment in a Fisher Sonic Dismembrator (Fisher Scientific) for 10 min at 60% power and then diluted to the desired concentration (3 wt%). The final NCC suspension was measured to have a zeta potential of -59 mV and a pH of 2.4.

Preparation of Chiral Nematic Mesoporous Silica (CNMS).

200 mL of a 3 wt% aqueous NCC suspension (the NCC used is sulfated and in the acid form, pH = 2.4) was sonicated for 30 min. The silica precursor, tetramethyl orthosilicate (TMOS, 8.0 mL, 54 mmol), was slowly added to the NCC suspension over 2 min with constant stirring. The mixture was then stirred until a homogeneous solution was obtained (30 min). This solution was divided into 10 mL portions, deposited into 60 mm x 15 mm polystyrene Petri dishes, and left to slowly evaporate at room temperature for about 48 h. After drying, free-standing NCC/silica composite films were obtained.

Removal of the NCC template was accomplished by treatment of the composite films (0.6 g) in 800 mL of 6 M hydrochloric acid at 80 °C for 18 h. To prevent excessive breakage of the film pieces, the samples were treated without stirring. After about 18 h, a brown suspension was obtained containing the silica film pieces. This was cooled to room temperature then carefully poured into excess cold water to dilute the acid. The silica film pieces were recovered

by vacuum filtration and rinsed with water. Upon drying, the films were visibly iridescent primarily in the blue, but appeared slightly discoloured. The film pieces were subsequently immersed in 300 mL of a chilled piranha solution (1:5 hydrogen peroxide: sulfuric acid) for approximately 5 min before quenching the reaction with water and further dilution. Free-standing chiral nematic mesoporous silica films with peak reflectance in the blue region of the visible spectrum were collected upon filtration.

Octyl functionalization of the Chiral Nematic Mesoporous Silica.

A batch of the CNMS films (300 mg) was prepared for octyl pore functionalization by heating the films under vacuum at just over 100 °C for 2 h to remove adsorbed water. The system was subsequently placed under nitrogen and the films were suspended in 5 mL of dry toluene. 1-(Triethoxysilyl)octane (0.79 mL, 2.51 mmol) was added via syringe, and the mixture was heated for 18 h at reflux (120 °C) under nitrogen. After cooling to room temperature, the functionalized film pieces were isolated by vacuum filtration and rinsed with chloroform to remove unreacted 1-(triethoxysilyl)octane. Upon drying, blue free-standing chiral nematic mesoporous silica films with octyl pore functionalization were obtained (CNMS-octyl). A water drop test indicated that these film pieces are hydrophobic.

Phenyl functionalization of the Chiral Nematic Mesoporous Silica.

A batch of the CNMS films (200 mg) was prepared for phenyl pore functionalization by heating the films under vacuum at just over 100 °C for 2 h to remove adsorbed water. The

system was subsequently placed under nitrogen and the films were suspended in 5 mL of dry toluene. Phenyltrimethoxysilane (0.312 mL, 1.67 mmol) was added via syringe, and the mixture was heated for 18 h at reflux (120 °C) under nitrogen. After cooling to room temperature, the functionalized film pieces were isolated by vacuum filtration and rinsed with chloroform to remove unreacted phenyltrimethoxysilane. Upon drying, blue free-standing chiral nematic mesoporous silica films with phenyl pore functionalization were obtained (CNMS-phenyl). A water drop test indicated that these film pieces are hydrophobic.

Liquid Crystal Loading of the Chiral Nematic Mesoporous Silicas.

The octyl functionalized and phenyl functionalized CNMS films were prepared for 5CB and 8CB loading by heating the films on a glass slide to just over 100 °C on a hot plate for 30 min. Next, 5CB or 8CB (warmed to 50 °C, above the transition temperatures into the isotropic phase) was added dropwise onto the film pieces with a micropipette. The films retained their blue coloration upon heating, but they became clear and colourless as the LC was introduced. Approximately 1 μL of LC was applied per 2-3 mg film piece of CNMS-octyl or CNMS-phenyl. These loaded films were left for 30 min at 50°C to allow the LC to fully diffuse throughout the pores. After this time the film pieces were cooled back to room temperature. If excess LC was visible on the surface of the thin film, this was removed mechanically either by wiping with a Kimwipe or by rinsing with warm water (heated to 45 °C). LC loaded octyl and phenyl functionalized CNMS (5CB@CNMS-octyl, 5CB@CNMS-phenyl, 8CB@CNMS-octyl, and 8CB@CNMS-phenyl) films were obtained with peak reflectance red-shifted from the original

blue to green or yellow. Unfunctionalized chiral nematic mesoporous silica film pieces were also loaded for comparison (5CB@CNMS and 8CB@CNMS).

Preparation of Ethylene-Bridged Chiral Nematic Mesoporous Organosilica (CNMO).

200 mL of a 3 wt% aqueous NCC suspension (the NCC used is sulfated and in the acid form, pH = 2.4) was sonicated for 30 min. The organosilica precursor, 1,2-bis(trimethoxysilyl)ethane (5.0 mL, 20 mmol), was slowly added to the NCC suspension over 2 min with constant stirring. The mixture was then stirred until a homogeneous solution was obtained (30 min). This solution was divided into 5 mL portions, deposited into 60 mm x 15 mm polystyrene Petri dishes, and left to slowly evaporate at room temperature for about 48 h. After drying, free-standing NCC/organosilica composite films were obtained (9.4 g total).

Removal of the NCC template was accomplished by treatment of the composite films (0.6 g) in 600 mL of 6 M sulfuric acid at 90 °C for 18 h. To prevent excessive breakage of the film pieces, the samples were treated without stirring. After about 18 h, a brown suspension was obtained containing the organosilica film pieces. This was cooled to room temperature then carefully poured into excess cold water to dilute the acid. The organosilica film pieces were recovered by vacuum filtration and rinsed with water. Upon drying, the films were visibly iridescent primarily in the blue, but appeared slightly discoloured. The film pieces were subsequently immersed in 300 mL of a chilled piranha solution (1:5 hydrogen peroxide: sulfuric acid) for approximately 5 min before quenching the reaction with water and further dilution. Free-standing ethylene-bridged chiral nematic mesoporous organosilica films with peak reflectance in the blue region of the visible spectrum were collected upon filtration.

Octyl functionalization of the Chiral Nematic Mesoporous Organosilica.

A batch of the CNMO films (100 mg) was prepared for octyl pore functionalization by heating the films under vacuum at just over 100 °C for 2 h to remove adsorbed water. The system was subsequently placed under nitrogen and the films were suspended in 5 mL of dry toluene. 1-(Triethoxysilyl)octane (0.30 mL, 0.95 mmol) was added via syringe, and the mixture was heated for 18 h at reflux (120 °C) under nitrogen. After cooling to room temperature, the functionalized film pieces were isolated by vacuum filtration and rinsed with chloroform to remove unreacted 1-(triethoxysilyl)octane. Upon drying, blue free-standing chiral nematic mesoporous organosilica films with octyl pore functionalization were obtained (CNMO-octyl). A water drop test indicated that these film pieces are hydrophobic.

Liquid Crystal Loading of the Chiral Nematic Mesoporous Organosilica.

The octyl-functionalized CNMO films were prepared for 8CB loading by heating the films on a glass slide to just over 100 °C on a hot plate for 30 min. Next, 8CB (warmed to 50 °C, above the transition temperature into the isotropic phase) was added dropwise onto the film pieces with a micropipette. The films retained their blue coloration upon heating, but they became clear and colourless as the LC was introduced. Approximately 1 μL of 8CB was applied per 2-3 mg film piece of CNMO-octyl. Immediately following introduction of the 8CB, a second glass slide was placed on top of the first to sandwich the film pieces. This setup was left for 30 min at 50°C to allow the 8CB to fully diffuse throughout the pores. After this time the glass slides were separated and the loaded film pieces were cooled back to room temperature. If excess 8CB was visible on the surface of the thin film, this was removed mechanically either by

wiping with a Kimwipe or by rinsing with warm water (heated to 45 °C). 8CB-loaded octyl-functionalized CNMO (8CB@CNMO-octyl) films were obtained with peak reflectance red-shifted from the original blue to green or yellow. Unfunctionalized chiral nematic mesoporous organosilica film pieces were also loaded for comparison (8CB@CNMO).

Characterization Techniques.

Ultraviolet-visible/near-infrared spectroscopy was conducted on a Cary 5000UV-Vis/NIR spectrophotometer. Transmission spectra were collected by mounting free-standing films so that the surfaces of the films were perpendicular to the beam path. The maximum transmittance was set to 100% in a region away from the reflectance peak. Variable temperature spectra were obtained using an Oxford Instruments OptistatDN Cryostat. Samples were prepared for study by sandwiching them between two 18 mm thickness 1 Fisherbrand glass cover slips and sealing the edges with 5 minute epoxy. Polarized optical microscopy (POM) was performed on an Olympus BX41 microscope. All images were taken with the polarizers in a perpendicular (crossed) arrangement. Variable temperature images were obtained with the use of an Instec hot stage. Thermogravimetric analysis was performed on a PerkinElmer Pyris 6 thermogravimetric analyser. Infrared spectra were obtained with a Nicolet 6700 FT-IR equipped with a Smart Orbit diamond attenuated total reflectance (ATR) attachment. X-ray diffraction spectra were collected using a D8 advance X-ray diffractometer with GADDS area detector. Gas adsorption studies were performed using a Micromeritics Accelerated Surface Area and Porosity (ASAP) 2000 system. Contact angle images were obtained with a mounted digital camera and analyzed using FTA32 software.

2.3 Results and Discussion

The chiral nematic mesoporous silica (CNMS) films and the ethylene-bridged chiral nematic mesoporous organosilica (CNMO) films used in this study as the liquid crystal host were synthesized in a similar manner to previously reported procedures.[40,41] Briefly, homogeneous mixtures of tetramethyl orthosilicate (TMOS) and NCC or 1,2-bis(trimethoxysilyl)ethane (BTMSE) and NCC were slowly dried to give free-standing composite films. The NCC templates were removed by acid hydrolysis in $HCl_{(aq)}$ or $H_2SO_{4(aq)}$, respectively, followed by a brief oxidative treatment in $H_2O_2/H_2SO_{4(aq)}$ to remove insoluble cellulosic by-products. The films retained a chiral nematic pore structure as evidenced by a strong selective reflection peak at approximately 440 nm for silica and 420 nm for organosilica.

I initially investigated the loading of 5CB and 8CB into the as-synthesized CNMS films. The liquid crystal was loaded into the films at elevated temperature as an isotropic liquid causing the initially iridescent films to become colorless. Upon cooling to room temperature, the films regained their iridescence with a red-shifted reflectance peak compared to the unloaded films. This red shift is caused by the increase in average refractive index after the incorporation of LC into the mesoporous films. These initial observations demonstrated that LC confined within CNMS films can be used to thermally switch their optical properties. Thermal switching of 5CB@CNMS and 8CB@CNMS was further studied by variable temperature polarized optical microscopy (POM, Figure 2-2). In both cases it was found that the LC-isotropic transition was very broad; the decrease in birefringence with increasing temperature was very gradual and some birefringence remained in both the LC-loaded films well above the nematic-isotropic transition

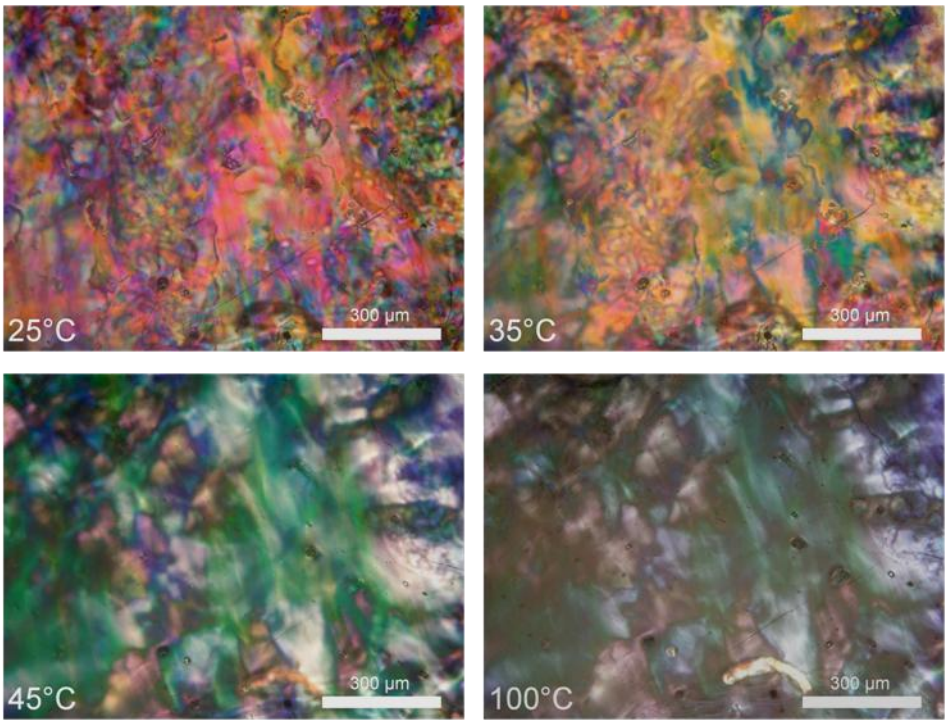

Figure 2-2. Variable temperature POM images of 5CB loaded unfunctionalized silica.

temperature of bulk 5CB (35 °C) and bulk 8CB (41 °C). This may be attributed to strong anchoring of 5CB and 8CB to the mesopore surface of CNMS as well as poor loading of the hydrophobic LC molecules into the hydrophilic organosilica. To improve the compatibility and switching of 5CB and 8CB within the mesoporous material, I functionalized CNMS with octyl groups and phenyl groups by reacting it with triethoxy(octyl)silane and phenyltrimethoxysilane to form CNMS-octyl and CNMS-phenyl, respectively. I postulated that this would improve LC loading by making the silica hydrophobic and facilitate the LC-isotropic transition by providing a more disordered mesopore surface. [82,83,84,85] Scheme 2-1 illustrates the preparation of the LC-loaded materials.

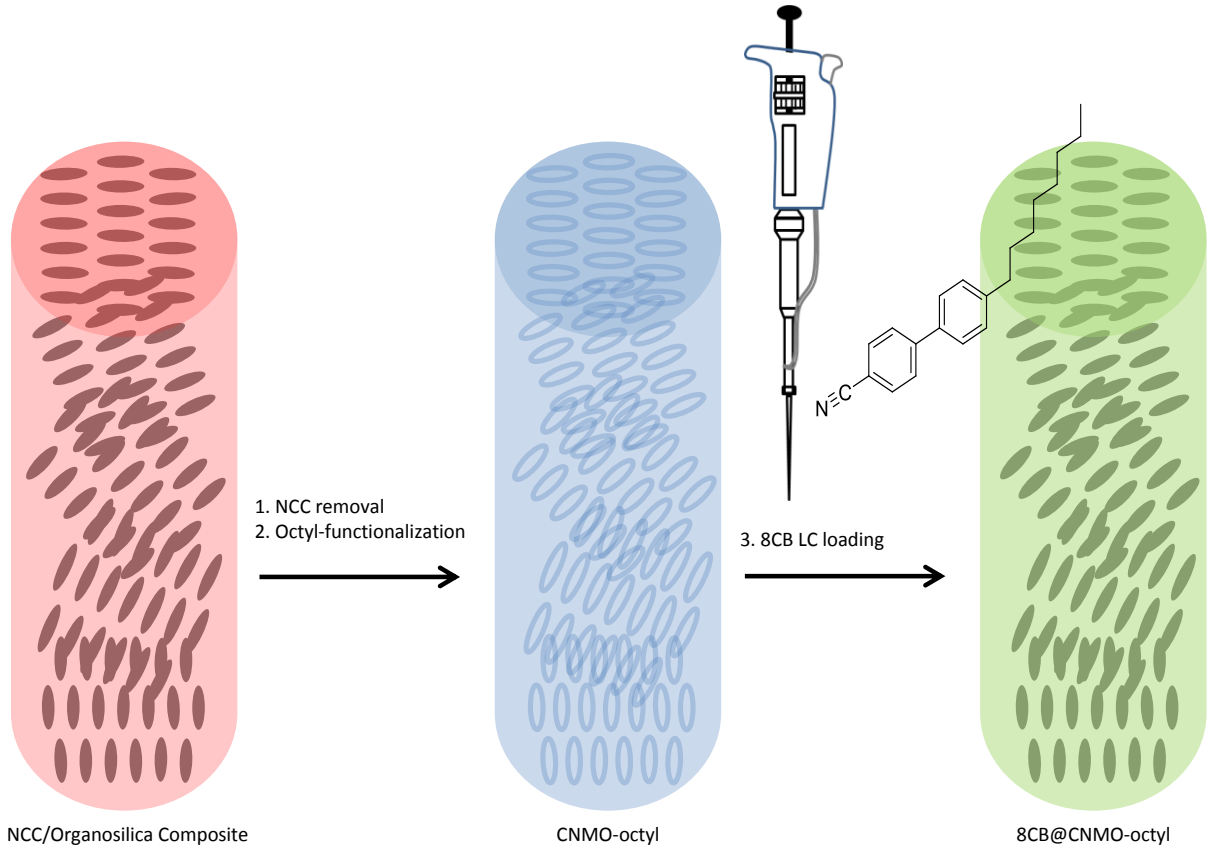

Scheme 2-1. Synthesis of the chiral nematic mesoporous organosilica composites used in this study.

Variable temperature POM on these samples showed a relatively sharp and reversible transition for all four composite materials (Figures 2-3, 2-4, 2-5, and 2-6). The octyl functionalized films appeared to have a more complete transition and full loss of birefringence in comparison to their phenyl functionalized counterparts, whether loaded with 5CB or 8CB. Additionally when comparing 5CB and 8CB loaded films, those loaded with 8CB had a sharper transition, occurring over a slightly shorter temperature range than those loaded with 5CB. Thus when continuing with this work I chose to work exclusively with 8CB loaded octyl functionalized films. Additionally, during the evolution of this work chiral nematic mesoporous organosilica was synthesized and identified to be easier to handle due to its less brittle nature and

resultant larger film piece size. As a result, only octyl functionalized organosilica loaded with 8CB was pursued with further investigations.

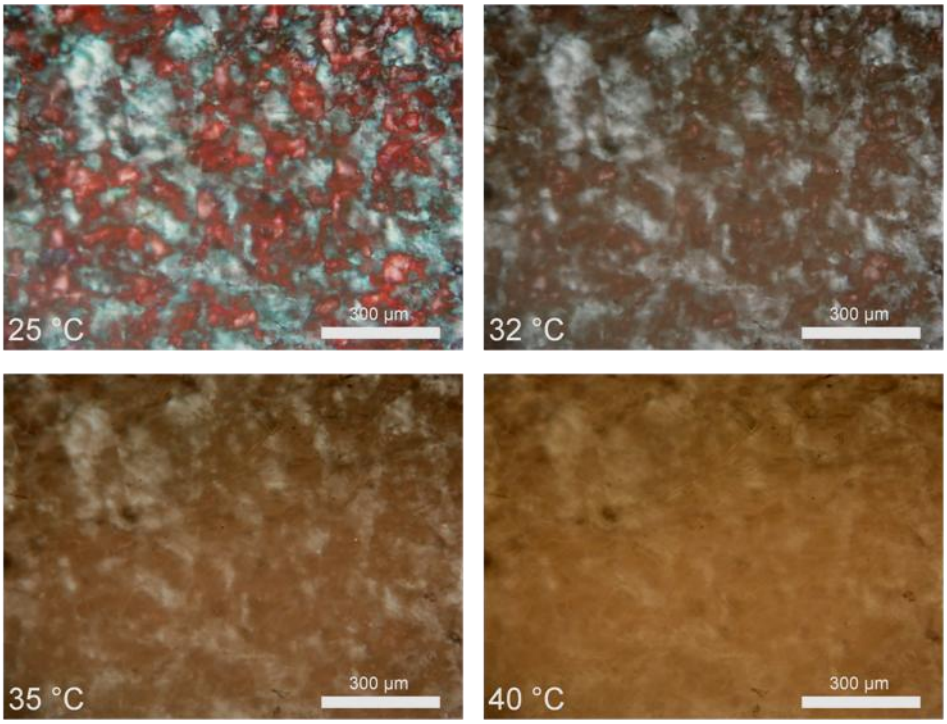

Figure 2-3. Variable temperature POM images of 5CB loaded octyl functionalized silica.

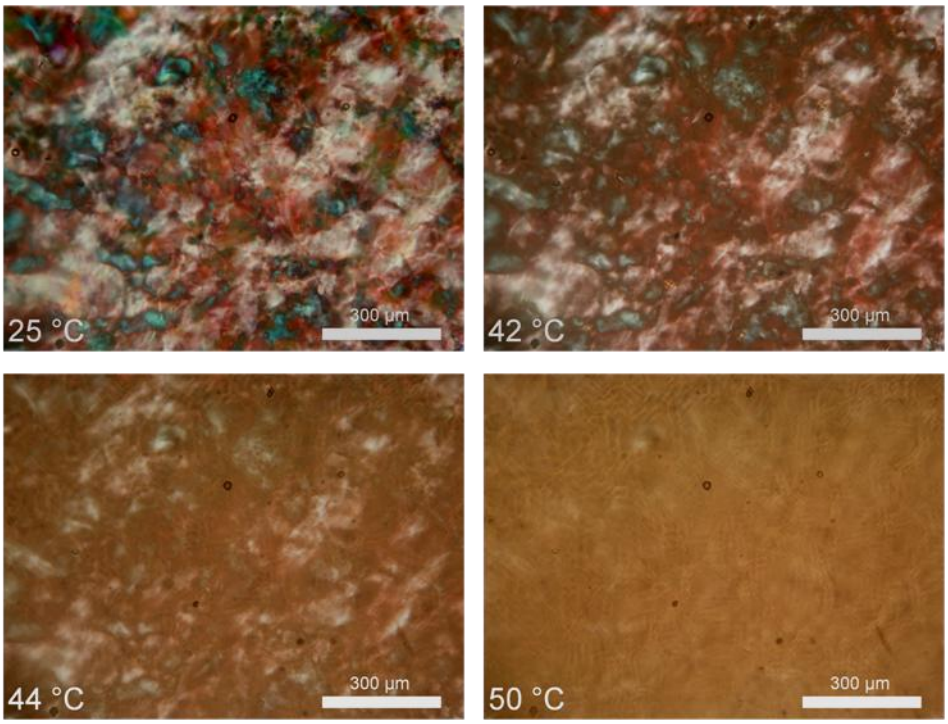

Figure 2-4. Variable temperature POM images of 8CB loaded octyl functionalized silica.

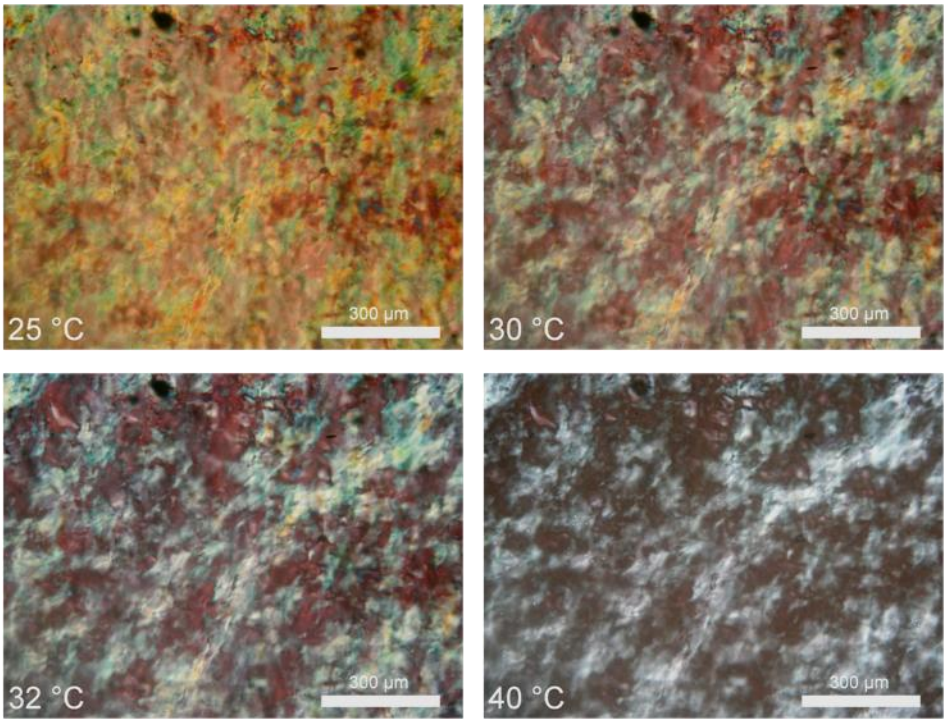

Figure 2-5. Variable temperature POM images of 5CB loaded phenyl functionalized silica.

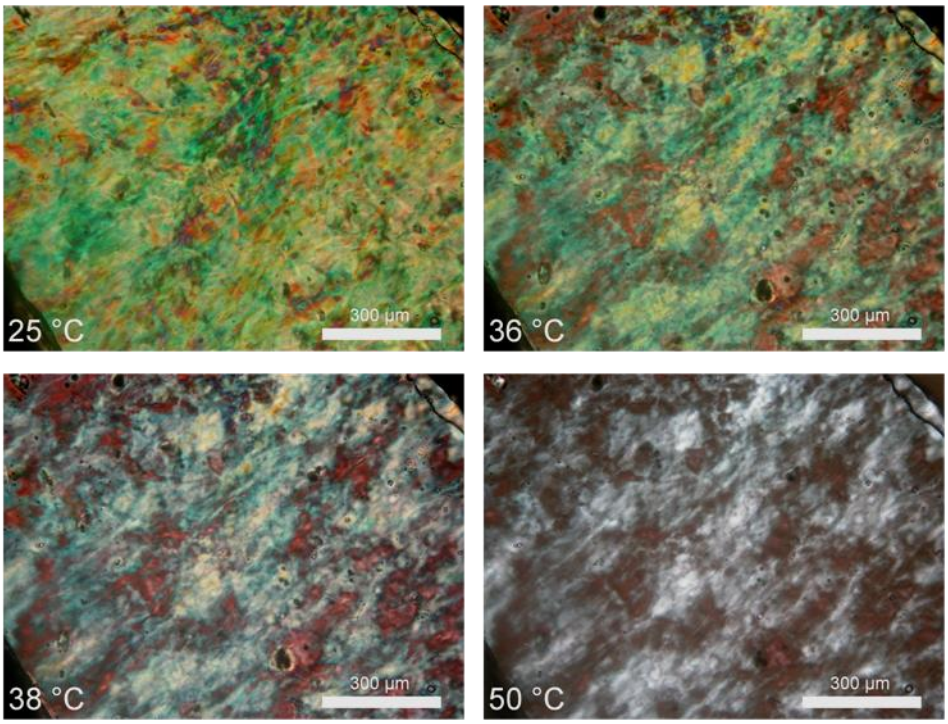

Figure 2-6. Variable temperature POM images of 8CB loaded phenyl functionalized silica.

The organosilica films were synthesized in a similar manner to their silica counterparts, but with an organosilica precursor, BTMSE, rather than TMOS. N_2 adsorption measurements were performed on CNMO films both before and after octyl functionalization. In both the original and subsequent octyl functionalized samples, type IV adsorption isotherms with type H2 hysteresis loops were observed (Figure 2-7). Brunauer-Emmett-Teller (BET) surface areas of 555 and 416 $m^2 g^{-1}$ and pore volumes of 1.3 and 0.96 $cm^3 g^{-1}$ were found for CNMO and CNMO-octyl, respectively. Fairly uniform Barret, Joyner, and Halenda (BJH) peak pore diameters of 7.1 nm and 4.7 nm were found for the CNMO and CNMO-octyl films, respectively. The decreased surface area, pore volume, and pore diameter are consistent with functionalizing the interior surface of the mesoporous organosilica with octylsilyl groups. Elemental analysis showed that the CNMO-octyl contained 22.44% C, and 4.19% H. This corresponds to approximately one

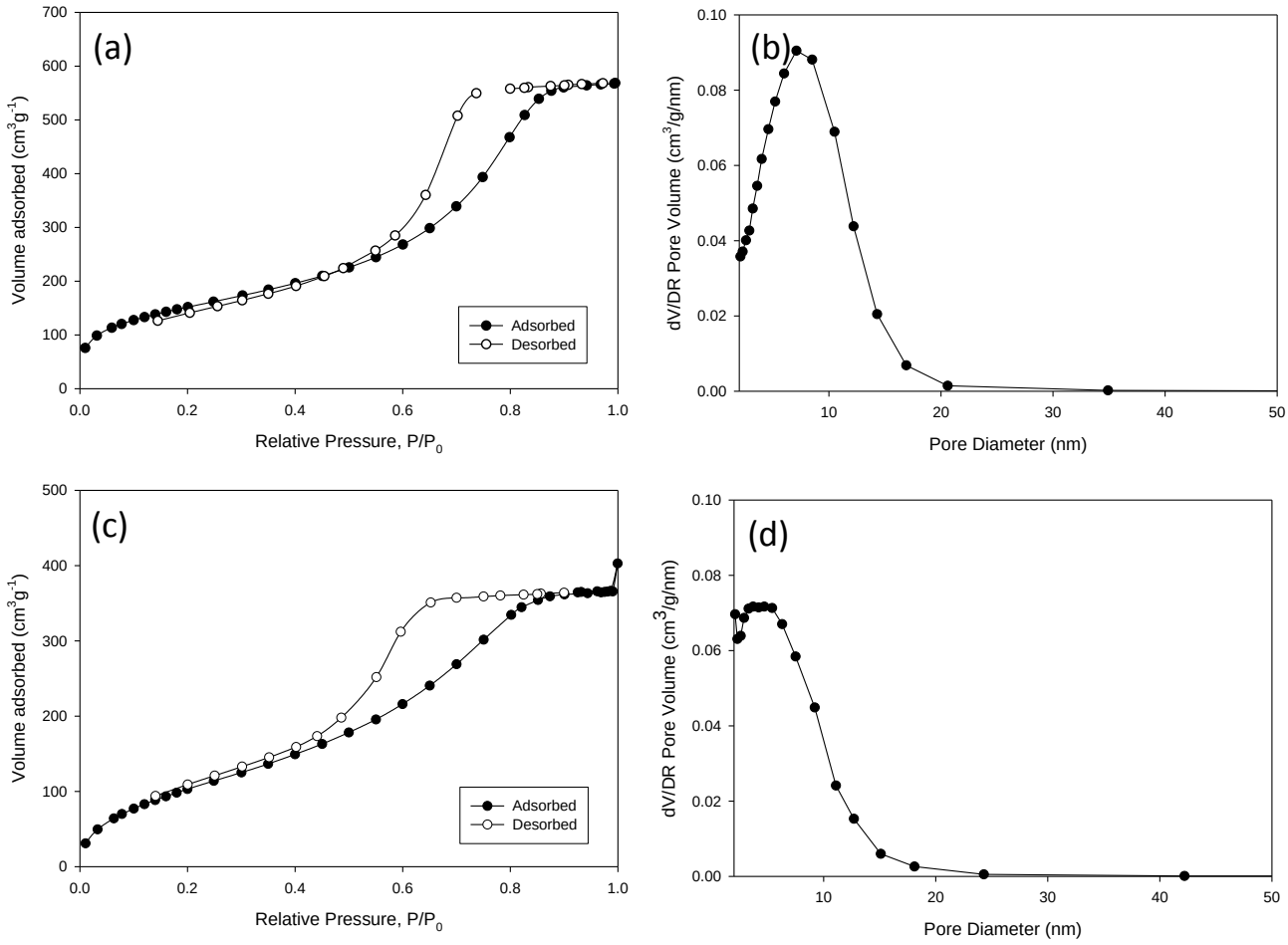

Figure 2-7. Brunauer-Emmett-Teller (BET) isotherms and Barret, Joyner, and Halenda (BJH) pore diameter distributions of chiral nematic mesoporous organosilica and octyl functionalized organosilica: (a) The type IV adsorption isotherm measured for a chiral nematic mesoporous organosilica film nematic mesoporous organosilica film (N_2/77 K). (b) The BJH pore size distribution for chiral nematic mesoporous organosilica film calculated from the adsorption branch of the isotherm. (c) The type IV adsorption isotherm measured for an octyl functionalized chiral nematic mesoporous organosilica film (N_2/77 K). (d) The BJH pore size distribution for octyl functionalized chiral nematic mesoporous organosilica film calculated from the adsorption branch of the isotherm.

octyl group per 10 ethyl groups in the structure.[a] Peaks were observed near 2900 cm^{-1} in the IR spectrum of the functionalized sample, which can be assigned to the C-H stretching mode of the alkyl chains. Additionally, octyl functionalization in the interior of the pores was confirmed by the change in optical properties of the material. There is a redshift in the peak reflectance wavelength of the chiral nematic structure, consistent with increasing the refractive index in the pores; this proves that the octyl functionalization occurs within the channels and not only on the exterior surface of the film. I performed contact angle measurements to prove that the octyl functionalized materials are hydrophobic (Figure 2-8). Before functionalization, the mesoporous organosilica films are hydrophilic, and upon exposure to water, the films become clear and colourless due to an approximate refractive index match between the organosilica walls and the water in the channels. A contact angle of approximately 28° was measured upon initial contact, which after a minute decreased by up to 25%. After octyl functionalization, addition of a drop of water to the films resulted in no change to the colour of the film. This verified that the films are hydrophobic. A contact angle of approximately 95° was measured upon contact with water, and after 1 minute only a slight change in angle could be noted (a decrease of 0-2 %).

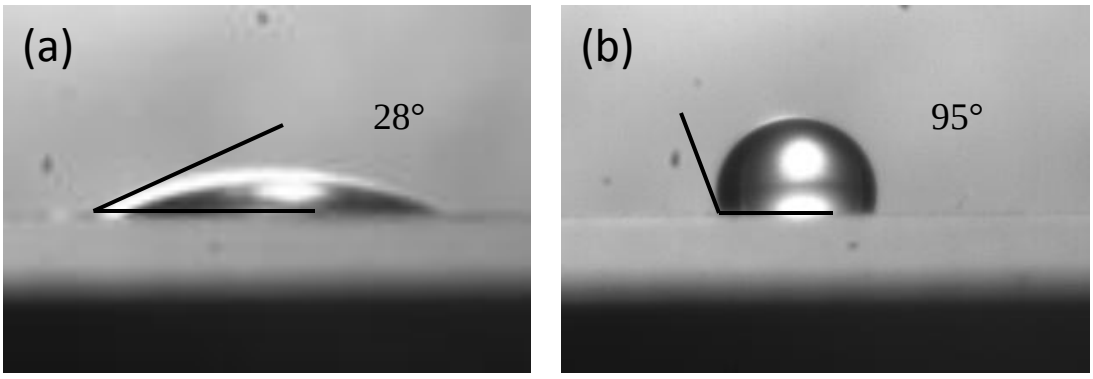

Figure 2-8. Contact angle images of (a) mesoporous organosilica and (b) octyl functionalized organosilica.

[a] Assuming a fully condensed structure with a formula of $[O_{1.5}SiCH_2CH_2SiO_{1.5}]_{10}[O_{1.5}SiC_8H_{17}]$ gives an analysis of 22.61% C and 3.86% H.

The 8CB liquid crystal was loaded into the octyl-functionalized organosilica (8CB@CNMO-octyl) at elevated temperature, when the LC was in the isotropic phase. Elemental analysis indicated that the CNMO-octyl films loaded with 8CB had 2.22% N, 46.08% C, and 6.14% H, by weight. This corresponds to about 27 wt% 8CB loaded in total.[b] This is in

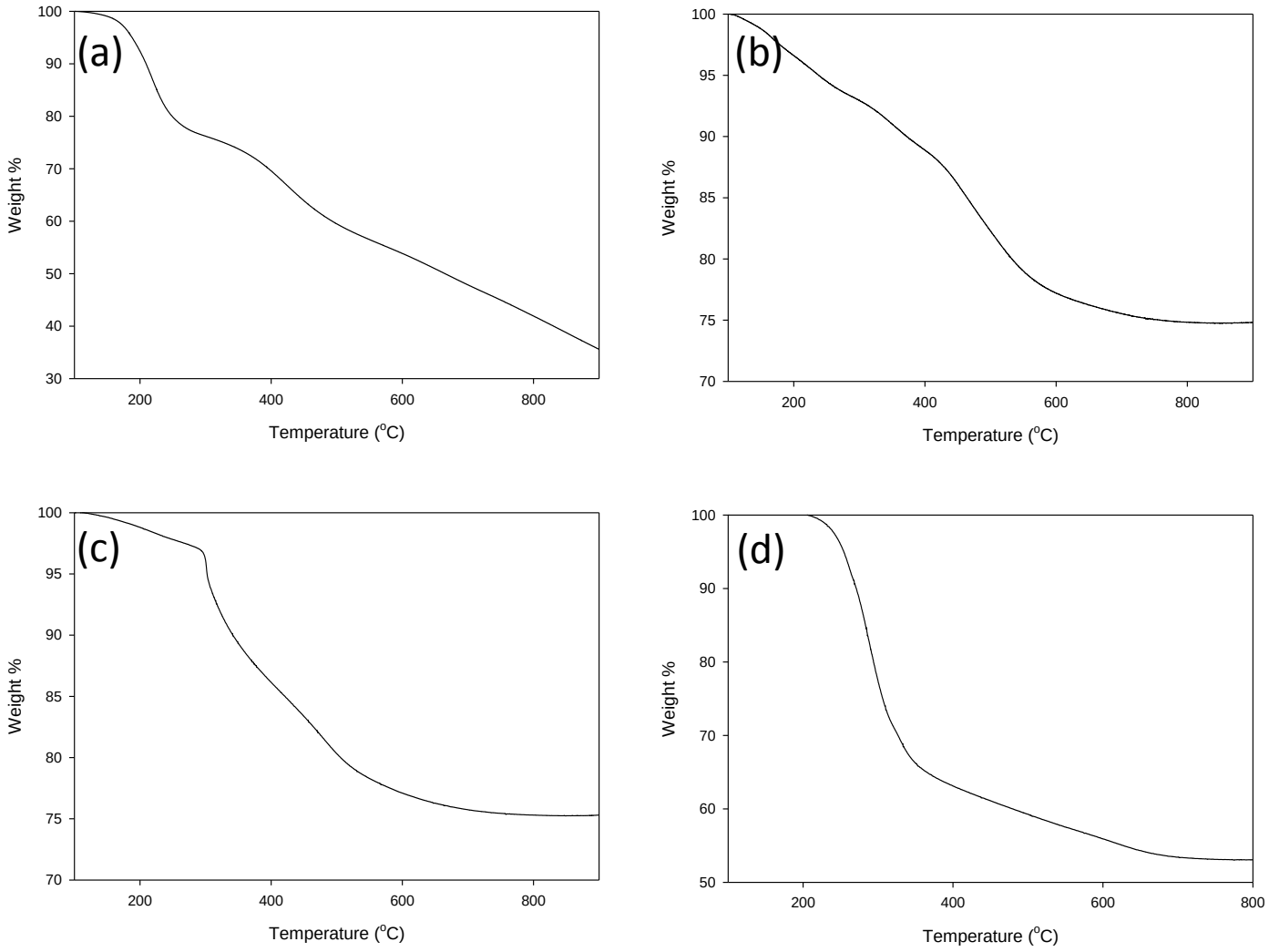

Figure 2-9. Thermogravimetric analysis (10 ℃ / min in air) of: (a) the NCC/organosilica composite film, (b) the mesoporous organosilica film, (c) the octyl functionalized organosilica film, and (d) the 8CB loaded octyl functionalized organosilica film.

[b] $[O_{1.5}SiCH_2CH_2SiO_{1.5}]_{10}[O_{1.5}SiC_8H_{17}][CN(C_6H_4)_2(CH_2)_7CH_3]_{1.384}$ gives an analysis of 46.08% C and 6.21% H.

agreement with the TGA data, which indicated the content to be approximately 30% by weight (Figure 2-9). IR data also confirms the uptake of 8CB into the films (Figure 2-10). An increase in intensity of the peaks near 2900 cm^{-1} corresponding to the C-H stretching mode of the alkyl

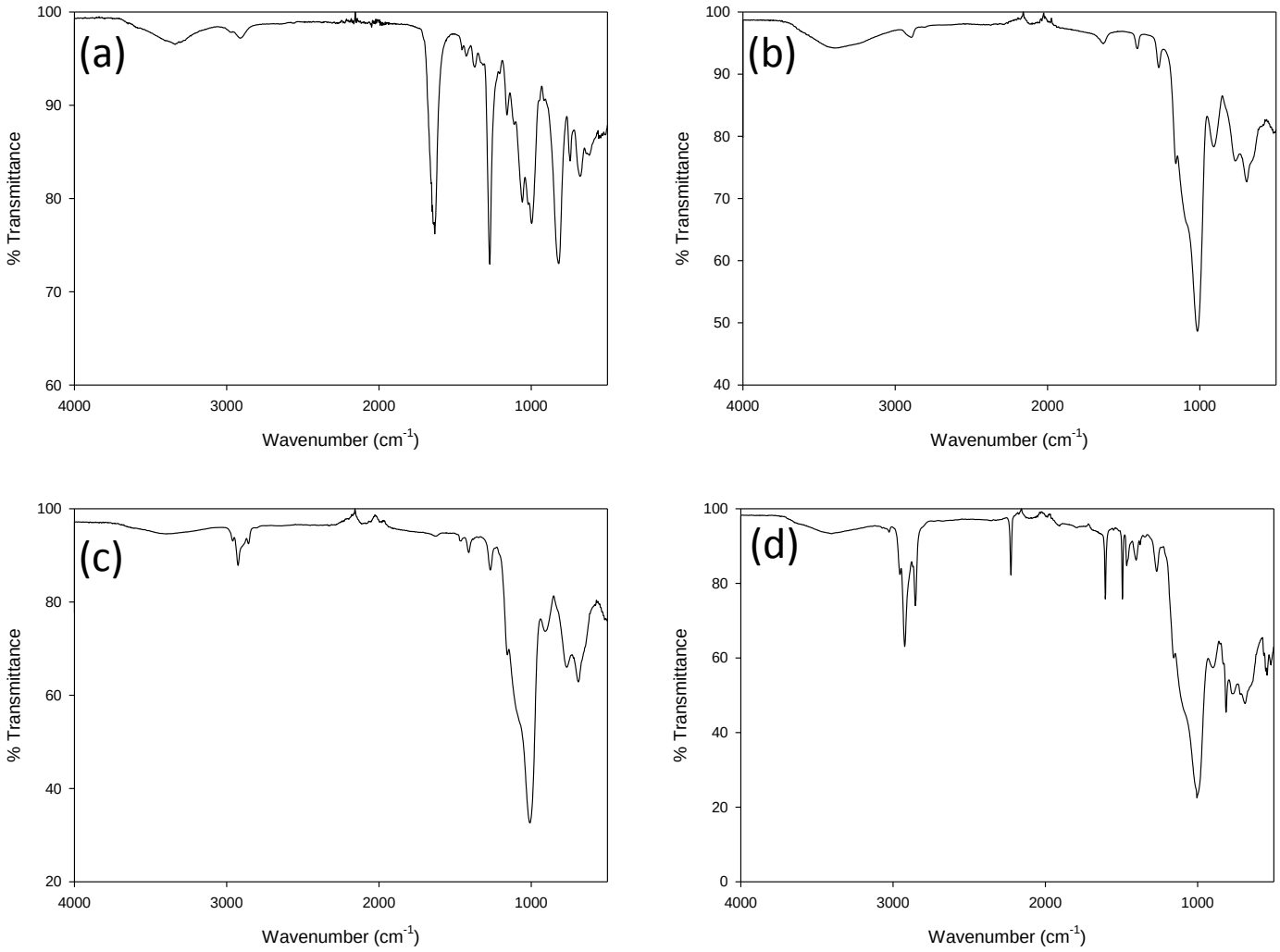

Figure 2-10. IR spectra of: (a) the NCC/organosilica composite film, (b) the mesoporous organosilica film, (c) the octyl functionalized organosilica film, and (d) the 8CB loaded octyl functionalized organosilica film.

chains is observed, as expected. The appearance of a peak at 2230 cm^{-1} and a pair of peaks near 1600 cm^{-1} and 1500 cm^{-1} that can be assigned to the CN stretching mode and benzene ring stretching modes of 8CB, respectively, further verifies the incorporation of 8CB into the films. X-ray diffraction (XRD) of the films after 8CB loading shows an increased intensity at about 20° 2-θ, where a broad, intense peak is observed for bulk 8CB at room temperature (Figure 2-11). This feature is consistent with nematic organization of 8CB within the mesopores of CNMO-octyl.

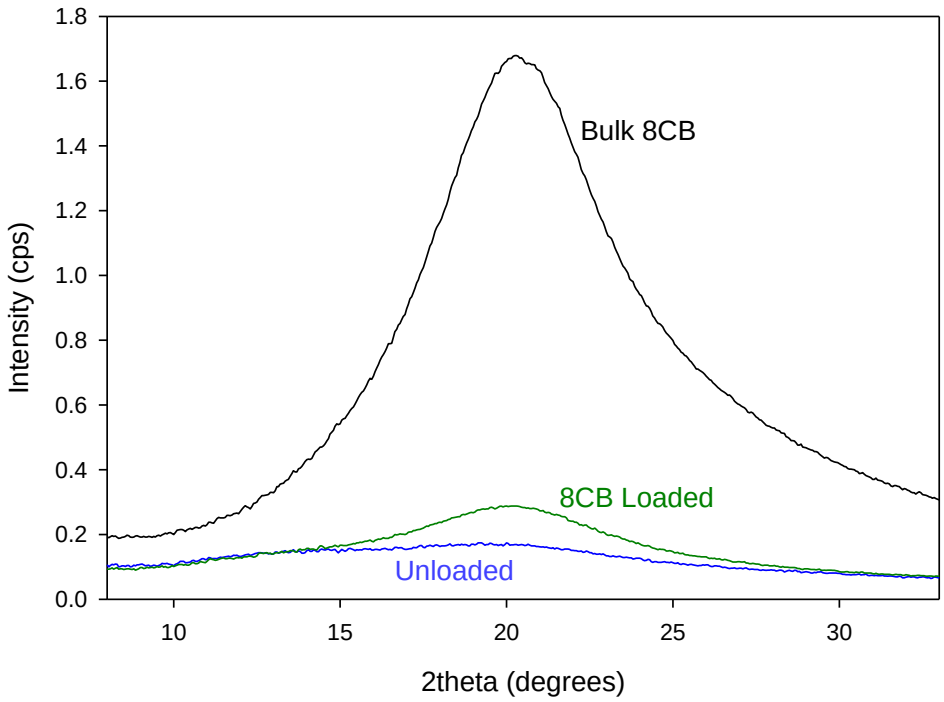

Figure 2-11. Overlaid X-ray diffraction patterns of the octyl functionalized organosilica film, the 8CB loaded octyl functionalized organosilica film, and bulk 8CB. There is a clear difference between the octyl functionalized free-standing mesoporous organosilica film with chiral nematic pore structure before and after loading with the liquid crystalline material, 8CB. The data for bulk 8CB is also displayed for comparison.

I studied the optical properties of the films before and after loading with 8CB by UV-visible spectroscopy. Figure 2-12 depicts the changes in peak reflected wavelength between the CNMO, CNMO-octyl, and 8CB@CNMO-octyl samples. For a chiral nematic structure, the peak reflected wavelength for incident light normal to the surface is given by Eqn. 1:

$$\lambda_{max} = n_{avg}P \quad (1)$$

where n_{avg} is the average refractive index of the material and P is the helical pitch of the chiral nematic structure.[16] The mesoporous organosilica films used in the current study typically display a reflectance peak at around 420 nm prior to octyl functionalization. After octyl

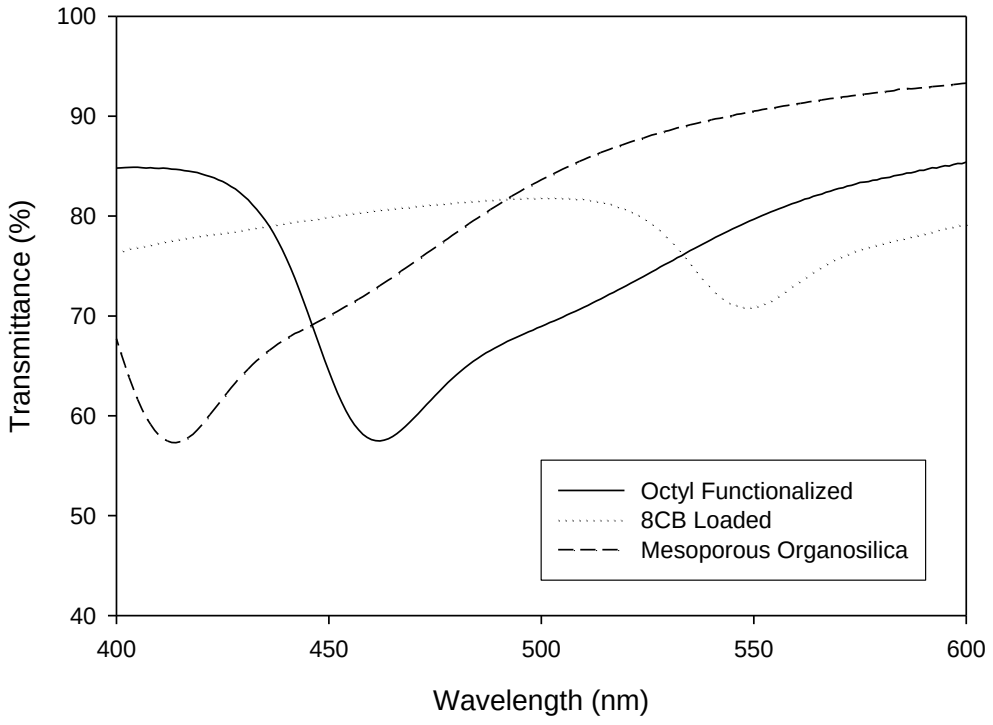

Figure 2-12. Overlaid UV-Vis spectra of the mesoporous organosilica film, the octyl functionalized organosilica film, and the octyl functionalized organosilica film loaded with 8CB. Note the small and then larger red shifts upon octyl functionalization and LC loading of the mesoporous organosilica, respectively.

functionalization, the color of the films does not change drastically, but there is a noticeable red shift in the UV-Vis spectrum. After loading the films with 8CB, however, a significant red shift of the reflection peak to ≈550 nm occurs causing the films to appear green in color. This red shift can be attributed to the change in n_{avg} brought about by the addition of 8CB, which can have a refractive index from 1.51 to 1.68 depending on liquid crystalline phase and optical axis.[86]

Each sample was examined by polarized optical microscopy (POM, Figure 2-13). All of the samples are birefringent and show textures similar to what has been previously observed for chiral nematic silica and organosilica films.[13,14] Different domains can be seen, but the overall texture remains similar between subsequent treatments. Furthermore, there is an apparent color change after each treatment that agrees with the overlaid UV-Vis spectra in Figure 2-12.

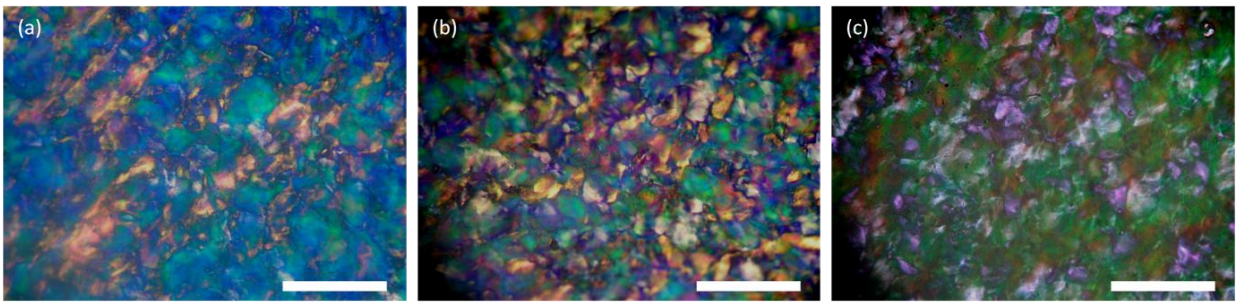

Figure 2-13. POM images of (a) the mesoporous organosilica film, (b) the octyl functionalized organosilica film, and (c) the 8CB loaded octyl functionalized organosilica film. All micrographs were taken with crossed polarizers (scale bar, 300 μm).

The main purpose of this work was to study the switching of 8CB within the free-standing octyl-functionalized organosilica films with chiral nematic pore structure, and to study the resulting change in optical properties of the host organosilica. When the films infiltrated with 8CB are heated to 40 °C, around the same temperature as the transition to isotropic for bulk 8CB, they visibly change in appearance, transforming from green and iridescent to clear and

colourless. Upon cooling, the loaded films return to their original iridescent, green state, indicating that the process is reversible. I studied this in greater detail using both variable temperature UV-Vis and POM experiments.

Figure 2-14 shows the overlaid UV-Vis spectra obtained at temperatures from room temperature (22 °C) to almost 60 °C in 5 degree intervals. This range was chosen in order to include the phase transition temperatures for the change in bulk 8CB from smectic to nematic, and nematic to isotropic (35 °C and 41 °C, respectively). From the UV-Vis measurements it is clear that a large increase in percent transmittance occurs between 37 °C and 42 °C, leaving only a small, barely detectable peak at the latter temperature. By the next measurement at 47 °C the peak has completely disappeared and does not change or return at higher temperatures. This phenomenon is reversible, and upon cooling back through the appropriate temperature range, the peak returns and increases back to its original intensity. A slight hysteresis in this reversal is apparent and could be due to confinement in the mesopores. This data is further supported by variable temperature POM images (Figure 2-15). At room temperature (22 °C) the loaded films are strongly coloured and birefringent. From room temperature to approximately 38 °C little change is detected; past 38 °C, however, some decrease in color intensity is observed. This decrease becomes more significant by 40 °C, and the colouration is completely lost by 42 °C.[c] This behavior is completely reversible, and no significant lag is apparent in the images. This response is very promising for a variety of different applications due to the ease and reversibility of the optical switching.[87,7]

[c] If the loaded films are heated much higher, 8CB can leach out of the pores.

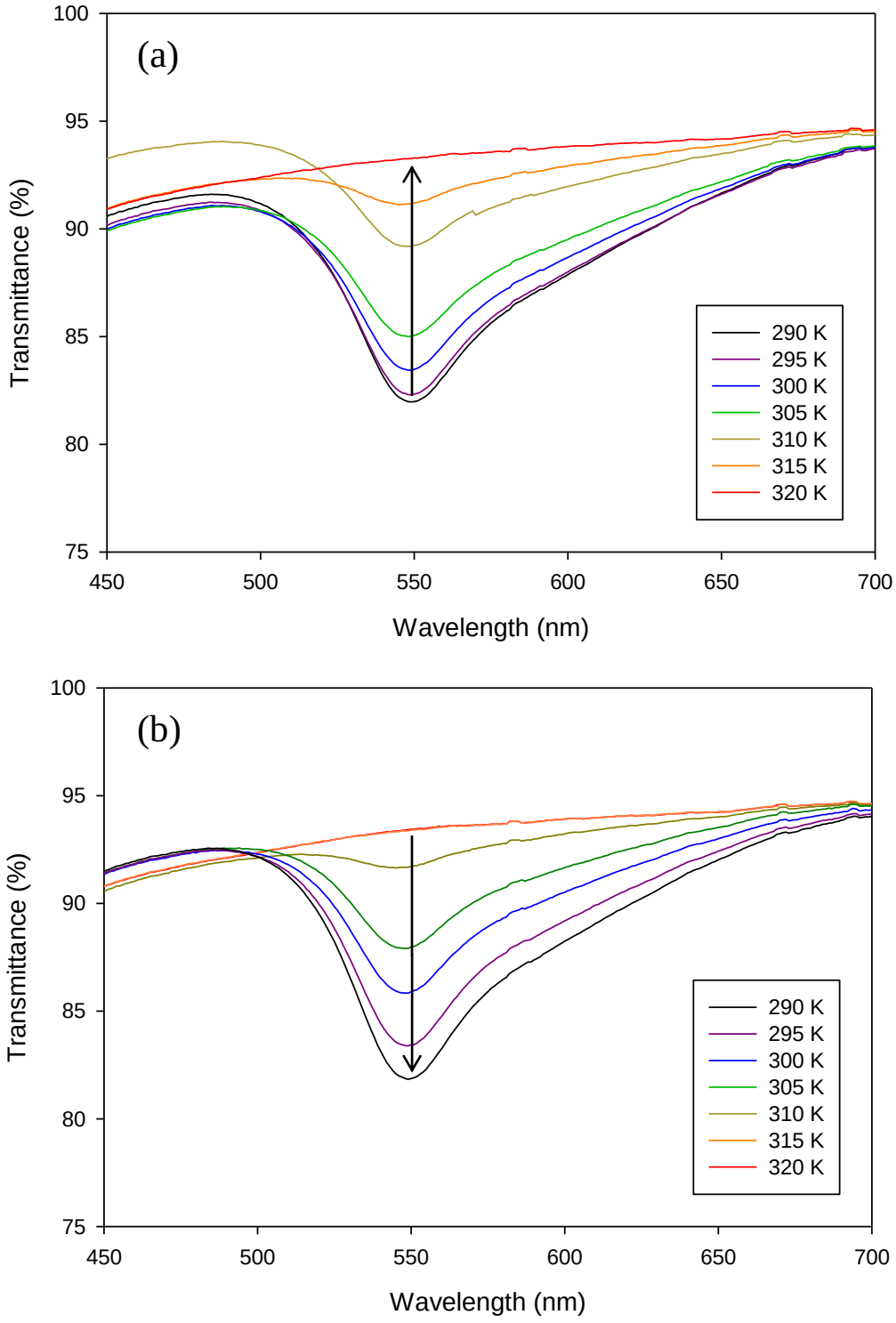

Figure 2-14. Normalized variable temperature UV-Vis spectra of an 8CB loaded octyl functionalized organosilica film. (a) Heating the film from 295 K to 330 K, with spectra recorded every 5 K. The peak at 550 nm decreases in intensity upon heating, with a large change from 310 K to 315 K, and completely disappears by 320 K. (b) Cooling the film from 330 K to 290 K, with spectra recorded every 5 K.

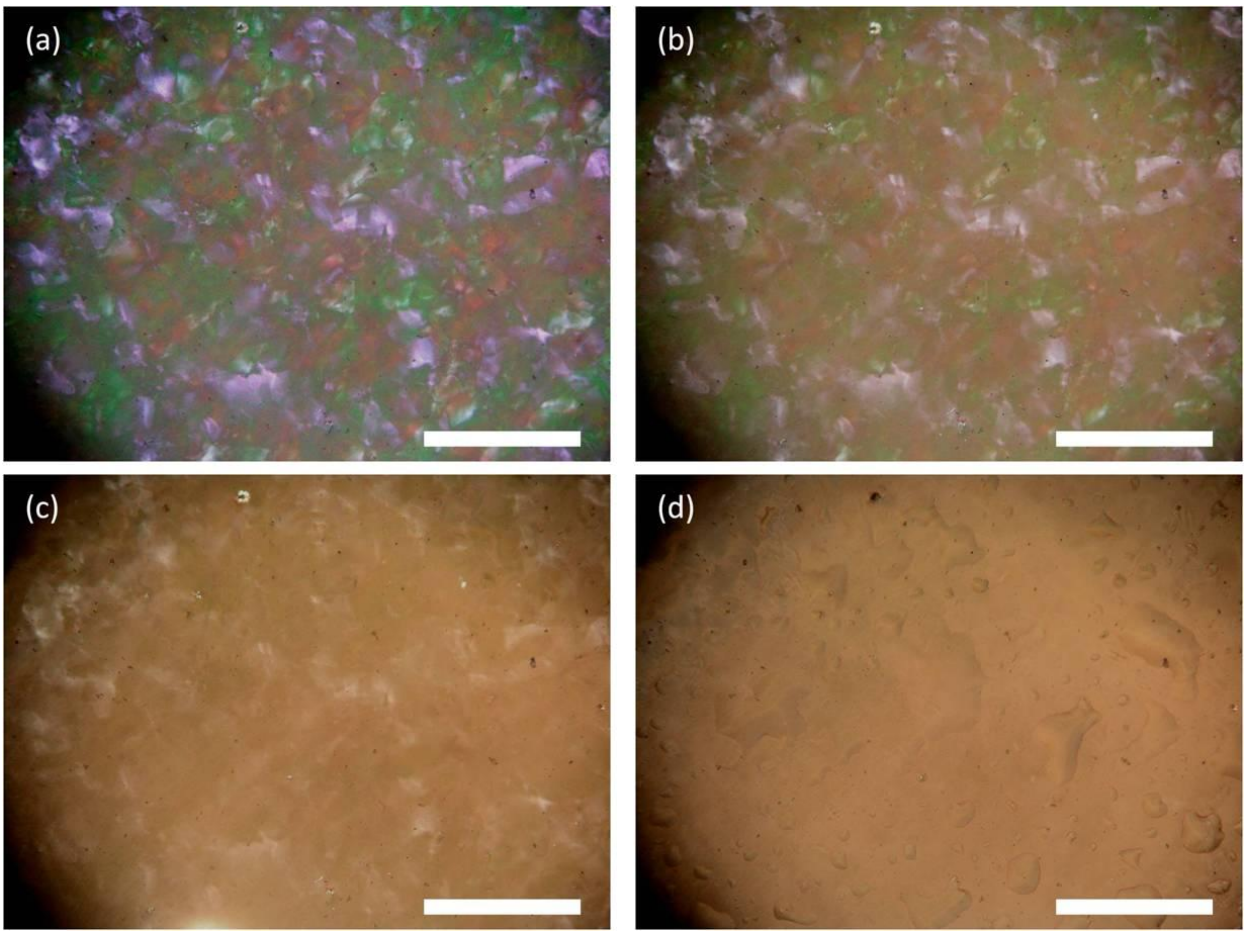

Figure 2-15. Variable temperature POM images of 8CB loaded octyl functionalized organosilica at: (a) 38 °C, (b) 40 °C, (c) 42 °C, and (d) 48 °C. Note the sharp transition over a few degrees, and the nearly complete loss of colour and birefringence from 38 °C to 42 °C. At higher temperatures (48 °C +) the 8CB liquid crystal can leach out of the pores. All micrographs were taken with crossed polarizers (scale bar, 300 μm).

The changes noted previously in our variable temperature experiments, both UV-Vis and POM, are indicative of a phase transition of the 8CB liquid crystal within the octyl functionalized organosilica pores. This temperature range found (≈38 °C to 42 °C) contains the transition temperature for 8CB in the bulk from the nematic to isotropic phases (41 °C). Although bulk 8CB displays a second transition at 35°C (smectic to nematic), this transition is not noted once the liquid crystal is confined within the pores; likely its geometry is too restrained by the 5 nm mesopores. The helical pores modify the organization of the 8CB liquid crystal and

it takes on a chiral nematic organization at room temperature. Upon heating above the nematic-isotropic transition temperature of 8CB, the film's colour and birefringence disappear, indicating a reorganization of the LC within the pores corresponding to a loss of order and transition to the isotropic phase. As demonstrated by the variable temperature UV-Vis and POM experiments described earlier, this transition is reversible.

This behaviour compares well with others in the literature. Bulk 8CB itself exhibits a sharp, reversible nematic to isotropic phase transition at 41 °C. Many studies involving altering its environment have been undertaken, which can demonstrate departures from bulk behaviour such as shifts in this temperature and broadening of the transition range. For example, the effect of 8CB film thickness and surface treatment have been examined; it was found that film thickness does have an effect on the nematic to isotropic phase shift temperature and that stress induced by surface orientation at the boundary led to a larger transition temperature shift than 8CB films of different thicknesses on untreated surfaces.[88] Confinement effects of *n*CB liquid crystals such as 8CB have been further studied by Iannacchione and coworkers.[89,90] They noted that although present when confined to macropores, the nematic to isotropic transition temperature shifts and there is an overall broadening of the phase transition. They showed that confinement had a much stronger effect on the smectic phase, which due to the deformation imposed by the pore walls had more difficulty in forming with decreasing pore size. Furthermore, when the liquid crystal was severely constrained by a porous network with an average pore diameter of ~7 nm, no distinct nematic to isotropic phase transition was observed at all, but rather a continuous, gradual decrease in local orientational order was observed with increasing temperature.

2.4 Conclusions

Loading of 5CB and 8CB into the unfunctionalized pores of chiral nematic mesoporous silica films and subsequent thermal cycling proved to be ineffective in producing an observable optical change in the composite material. Preliminary work with octyl and phenyl functionalized CNMS loaded with 5CB and 8CB established that the sharpest and most complete thermally reversible transition was found with 8CB loaded octyl functionalized silica films. This led to expansion of this work with the more flexible organosilica counterpart. It was demonstrated that hydrophobic octyl functionalized CNMO is an excellent host for the liquid crystal 8CB. The helical pore structure of the organosilica host enforces a chiral nematic organization on a non-chiral nematic liquid crystal without the use of a chiral dopant. Variable temperature UV-Vis and POM studies showed that the 8CB/organosilica composite material undergoes sharp and thermally-reversible optical switching at a temperature that correlates well with the liquid crystalline to isotropic transition of bulk 8CB. This approach should be expandable to other nematic liquid crystals, which will allow for the thermal response of the CNMO films to be readily tuned. The use of stimulus-induced switching of a guest to modify the optical properties of a mesoporous host may have possible applications in the development of dynamically switchable devices in displays or sensors.

Chapter 3: Azobenzene Doped Liquid Crystal Loading

3.1 Introduction

The azobenzene (AB) molecule is composed of two phenyl rings linked by a nitrogen-nitrogen double bond.[91] Derivatives of azobenzene encompass a wide class of molecules, which include the core azobenzene structure with different functional groups extending from the phenyl rings. These compounds are strongly coloured due their absorption of light and are consequently widely used as dyes in a variety of industrial applications.[1,92] Azobenzene and its derivatives can exist as two different isomers, trans and cis.[93] The cis isomer is less stable than the trans isomer due to the increased steric bulk of the distorted configuration and less delocalization of electrons. Thus, in the ground state, the molecule will reside in the trans configuration, but interconversion of the two can be accomplished by photoisomerization.[94] The exact wavelength at which azobenzene isomerisation occurs depends on the specific structure of each azobenzene derivative molecule. Different substitutions of the phenyl groups result in azobenzene derivatives that range from yellow to orange to red owing to subtle differences in their electronic absorption spectra.[2] Ultraviolet (UV) light, which corresponds to the energy gap of the π-π^* transition, typically 300-400 nm, causes the trans to cis conversion, whereas visible light, >400 nm, which corresponds to the energy gap of the n-π^* transition or thermal relaxation will cause the molecule to revert back to the trans form (Figure 3-1).[95] The photoisomerization of azobenzene is fast, occurring on the timescale of picoseconds, while the rate of thermal relaxation is much slower. This rate can greatly vary from compound to compound, but can often require several hours.

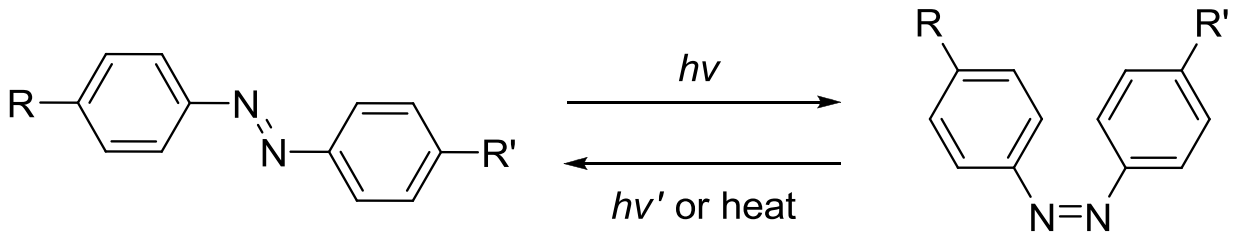

Figure 3-1. Generic azobenzene photoisomerization.

The light-induced molecular motion from the photoisomerization of azobenzene and its derivatives can be harnessed to do work on larger scales. For instance, polymeric materials containing an azobenzene moiety can reversibly deform and selective irradiation can result in patterning.[96,97] Additionally, either when directly incorporated or doped in to a LC film, azobenzene photoisomerisation can cause a switch to the phase of the material (Figure 3-2).[98,99]

In this work, the objective was to modify the reflectivity of the organosilica films by infiltrating the mesopores with another stimulus-responsive guest. An azobenzene derivative, diazene, 1-(4-butylphenyl)-2-(4-methoxyphenyl) (ABD), was selected for infiltration as a dopant in 8CB due to its relatively facile synthesis and compatible solubility (Figure 3-3). In the following, LC/ABD mixtures of 1%, 5%, and 10% dopant by volume were prepared (8CB/ABD-1%, 8CB/ABD-5%, and 8CB/ABD-10%) and then loaded into octyl functionalized chiral nematic mesoporous organosilica. These new composite materials retained iridescence; however they also acquired the intense brown-orange colour of the azobenzene derivative. The materials were then examined for their response to 365 nm irradiation and subsequent thermal and visible light induced relaxation, and showed varying degrees of change by POM and UV-vis spectroscopy. This behaviour could potentially be harnessed for applications such as in sensing or patterning.

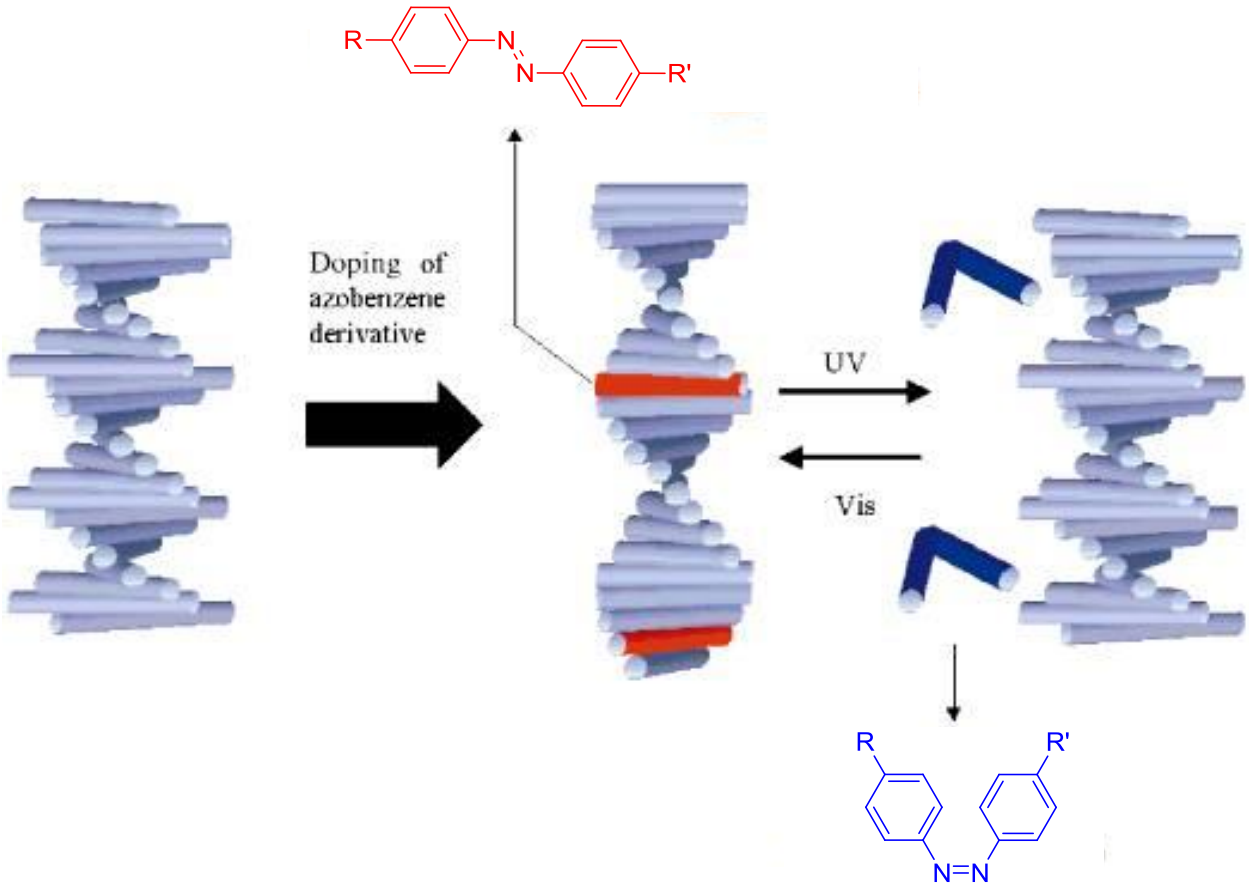

Figure 3-2. Schematic of the doping of a rod-shaped liquid crystal with an azobenzene dopant. The straight, red rods represent the azobenzene dopant in the trans configuration, while the bent, blue rods represent the azobenzene dopant in the cis configuration. Reproduced with permission from reference 7. Copyright 2001 John Wiley and Sons.

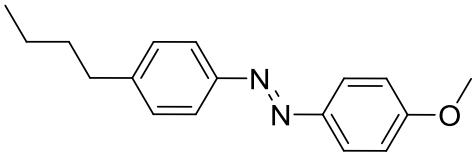

Figure 3-3. Chemical structure of the azobenzene derivative, diazene, 1-(4-butylphenyl)-2-(4-methoxyphenyl) (ABD).

3.2 Experimental

Materials.

8CB was obtained from Synthon Chemicals. DCM (≥ 99.5 %), acetone (≥ 99.5 %), and chloroform (≥ 99.8 %) were used as received from Sigma Aldrich or further diluted where specified. Potassium carbonate, K_2CO_3, and sodium sulfate, Na_2SO_4, both certified anhydrous, were purchased from Fisher Scientific. Iodomethane, CH_3I, was purchased from Sigma Aldrich. Deuterated solvents were purchased from Cambridge Isotope Laboratories, Inc. Diazene, 1-(4-butylphenyl)-2-(4-hydroxyphenyl) was synthesized by a fellow group member according to literature procedures.

Synthesis of diazene, 1-(4-butylphenyl)-2-(4-methoxyphenyl).

Diazene 1-(4-butylphenyl)-2-(4-hydroxyphenyl) (1.06 g, 4.13 mmol) was dissolved in 100 mL of acetone. A molar excess of K_2CO_3 (2 g, 6 mmol) was added to the solution. Iodomethane (388 μL, 6.23 mmol) was then added dropwise with stirring. The reaction mixture was left at reflux (60 °C) for 18 h. After that time had elapsed, the reaction mixture was removed from the heat and allowed to cool. The solvent was removed by rotary evaporation and the remaining residue was partitioned between water (200 mL) and DCM (200 mL). The organic layer was collected and set aside, while the aqueous layer was further extracted with three 75 mL portions of DCM. The combined organic layers were dried with Na_2SO_4, vacuum filtered, and

concentrated by rotary evaporation. Diazene, 1-(4-butylphenyl)-2-(4-methoxyphenyl) (ABD), a viscous, dark orange/brown liquid was obtained.[d]

^{1}H NMR (400 MHz, $CDCl_3$): δ (ppm) 7.96 (d, *J* = 9.14 Hz, 2H, aromatic C*H*), 7.86 (d, *J* = 8.22 Hz, 2H, aromatic C*H*), 7.34 (d, *J* = 8.22 Hz, 2H, aromatic C*H*), 7.04 (d, *J* = 8.83 Hz, 2H, aromatic C*H*), 3.89 (s, 3H, OCH_3), 2.72 (t, *J* = 7.61 Hz, 2H, CH_2), 1.68 (quin, *J* = 7.61 Hz, 2H, CH_2), 1.34 - 1.51 (m, 2H, CH_2), 0.99 (t, *J* = 7.31 Hz, 3H, CH_3); ^{13}C NMR (100 MHz, $CDCl_3$): δ (ppm) 161.8, 150.9, 145.7, 129.0, 124.5, 122.5, 114.1, 77.3, 77.0, 76.7, 55.5, 35.5, 33.4, 22.3, 13.9; IR (neat): υ = 2956, 2929, 2857, 1599, 1584, 1500, 1249, 1152, 1140, 1030, 836, 555 cm^{-1}.

Preparation of the LC/Dopant Mixtures.

Three different 100 μL liquid crystal/azobenzene dopant (LC/ABD) samples were prepared by mixing 99 μL 8CB with 1 μL azobenzene dopant, 95 μL 8CB with 5 μL azobenzene dopant, and 90 μL 8CB with 10 μL azobenzene dopant, resulting in 1%, 5%, and 10% v/v doped mixtures, respectively. The samples were prepared by combining the appropriate amounts of 8CB (warmed to 50 °C, above the transition temperature into the isotropic phase) and diazene, 1-(4-butylphenyl)-2-(4-methoxyphenyl) in chloroform (15 mL). The resultant mixtures were heated to 50 °C with stirring for 1.5 h. After this time, the mixtures were allowed to cool and concentrated by rotary evaporation, yielding the final 1%, 5%, and 10% v/v doped mixtures (8CB/ABD-1%, 8CB/ABD-5%, and 8CB/ABD-10%). They appeared orange in colour, darker orange with higher concentrations of the dopant, and their consistency closely resembled the phase at the corresponding temperature of their primary component, 8CB.

[d] Although this compound is available from Aldrich, it is expensive so I prepared it myself.

Preparation of the Loaded Films.

The octyl functionalized CNMO films were prepared for LC/ABD loading by heating the films on a glass slide to just over 100 °C on a hot plate for 30 min. Next, the LC/ABD mixtures (warmed to 50 °C, above the transition temperature of 8CB into the isotropic phase) were added dropwise onto the film pieces with a micropipette. The films retained their blue coloration upon heating, but they lost their iridescence and became strongly orange coloured after the LC/ABD mixtures were introduced. Approximately 1 μL of each mixture was applied per 2-3 mg film piece of CNMO-octyl. Immediately following introduction of the LC/ABD mixtures, a second glass slide was placed on top of the first to sandwich the film pieces. This setup was left for 30 min at 50°C to allow the mixtures to fully diffuse throughout the pores. After this time the glass slides were separated and the loaded film pieces were cooled back to room temperature. If excess LC/ABD mixture was visible on the surface of the thin films, this was removed mechanically by wiping with a Kimwipe. 8CB/ABD loaded octyl functionalized CNMO (8CB/ABD-1%@CNMO-octyl, 8CB/ABD-5%@CNMO-octyl, and 8CB/ABD-10%@CNMO-octyl) films were obtained that still displayed iridescence, but were also strongly coloured orange. Unfunctionalized chiral nematic mesoporous organosilica film pieces were also loaded for comparison (8CB/ABD-1%@CNMO, 8CB/ABD-5%@CNMO, and 8CB/ABD-10%@CNMO).

Characterization Techniques.

Ultraviolet-visible/near-infrared spectroscopy was conducted on a Cary 5000UV-Vis/NIR spectrophotometer. Transmission spectra were collected by mounting free-standing

films so that the surfaces of the films were perpendicular to the beam path. The maximum transmittance was set to 100% in a region away from the reflectance peak. Polarized optical microscopy (POM) was performed on an Olympus BX41 microscope. All images were taken with the polarizers in a perpendicular (crossed) arrangement. Infrared spectra were obtained with a Nicolet 6700 FT-IR equipped with a Smart Orbit diamond attenuated total reflectance (ATR) attachment. 400 MHz ^{1}H NMR and 100 MHz ^{13}C NMR spectra were recorded on a Bruker AV-400 spectrometer.

3.3 Results and Discussion

The azobenzene dopant, diazene, 1-(4-butylphenyl)-2-(4-methoxyphenyl) (ABD), was synthesized by methylation of diazene, 1-(4-butylphenyl)-2-(4-hydroxyphenyl) (Scheme 3-1)[100] with a reasonably good yield (~80%). The viscous, brown liquid that was obtained did not require any further purification as seen by the ^{1}H NMR (Figure 3-4), ^{13}C NMR (Figure 3-5), and IR (Figure 3-6) spectra of the crude product. LC/ABD mixtures were prepared in concentrations of 1, 5, and 10 volume percent dopant by heating them in chloroform. These were then loaded into octyl functionalized chiral nematic mesoporous organosilica films to give 8CB/ABD-1%@CNMO-octyl, 8CB/ABD-5%@CNMO-octyl, and 8CB/ABD-10%@CNMO-octyl. These films retained their iridescence upon loading, however they were also strongly coloured orange due to the azobenzene dopant (Figure 3-7). Additionally, three other samples were prepared for comparison by loading the LC/ABD into non functionalized chiral nematic mesoporous organosilica to give 8CB/ABD-1%@CNMO, 8CB/ABD-5%@CNMO, and 8CB/ABD-10%@CNMO.

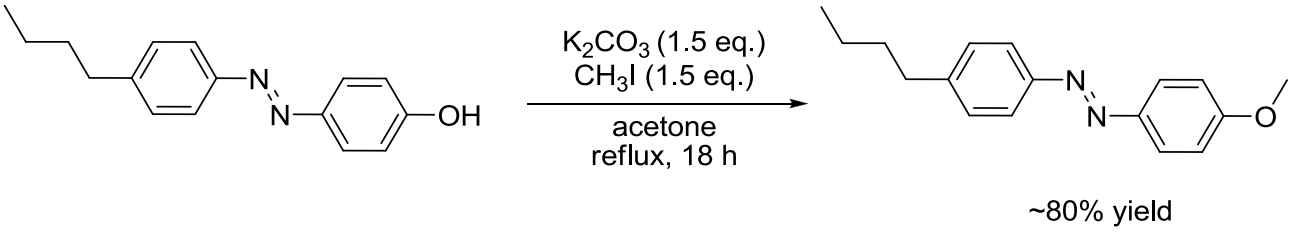

Scheme 3-1. Synthesis of the azobenzene dopant.

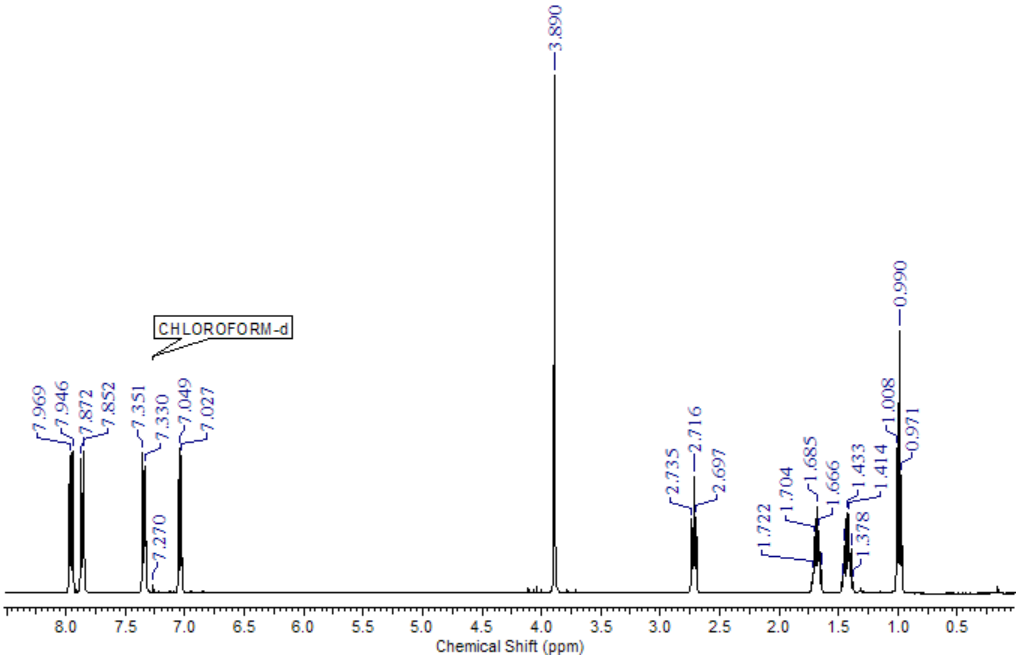

Figure 3-4. ^{1}H NMR spectrum (400 MHz, $CDCl_3$) of the azobenzene dopant.

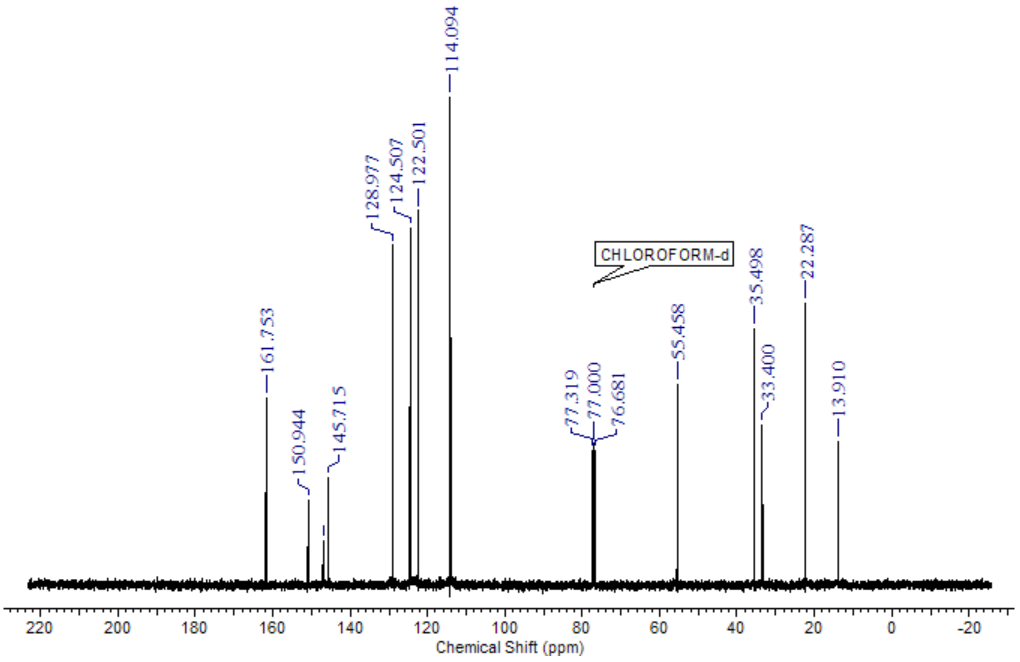

Figure 3-5. ^{13}C NMR spectrum (100 MHz, $CDCl_3$) of the azobenzene dopant.

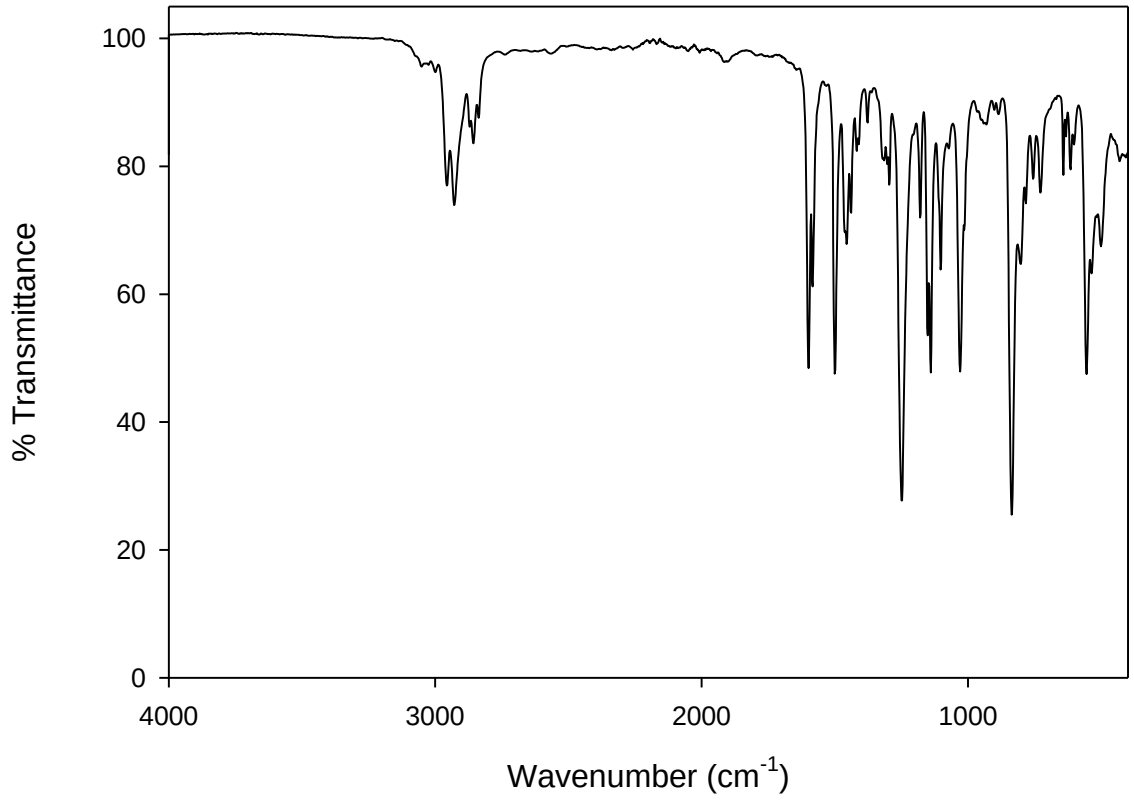

Figure 3-6. IR spectrum of the azobenzene dopant.

POM images of the films after loading (Figure 3-8) show that birefringence is retained in the octyl functionalized samples; however the birefringence of the non functionalized samples is greatly diminished. Irradiation at 365 nm proved to have an effect on the loaded films. After 2 minutes of irradiation they appeared to have lost iridescence and inspection by POM showed a

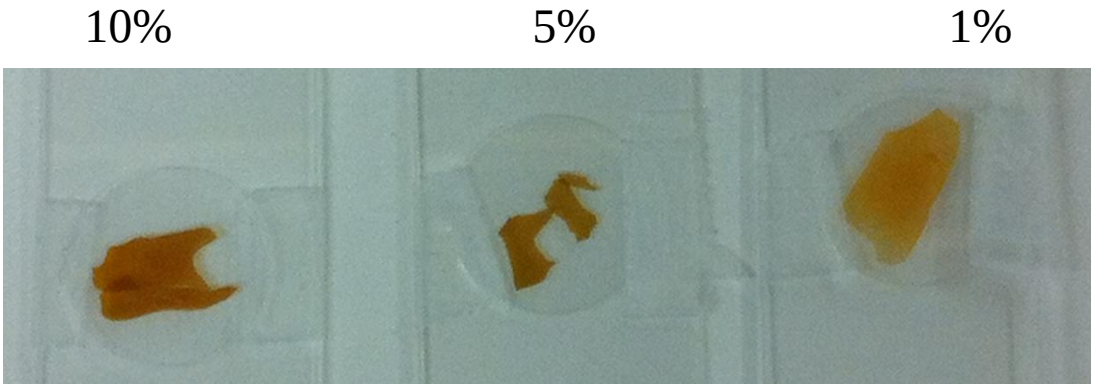

Figure 3-7. Photographs of CNMO-octyl films loaded with azobenzene doped 8CB.

significant loss of birefringence as well (Figure 3-9). The film pieces loaded with the LC/ABD of highest ABD percent (8CB/ABD-10%) showed a more complete transition than the films with 8CB/ABD-5%. The 8CB/ABD-1% loaded films showed little if any change after irradiation. This would follow since it is the deformation of the azobenzene derivative dopant which destabilizes the liquid crystalline phase and causes the transition to isotropic. When the molecule is in the trans form, it is relatively linear and packs nicely with the chiral nematic phase of the 8CB within the pores. Upon irradiation, however, the molecule isomerizes to the bent cis form and destabilizes this packing. If enough dopant is present, as is the case with 5% and even more so with 10% dopant by volume, this destabilization is sufficient to cause an overall phase change within the films.

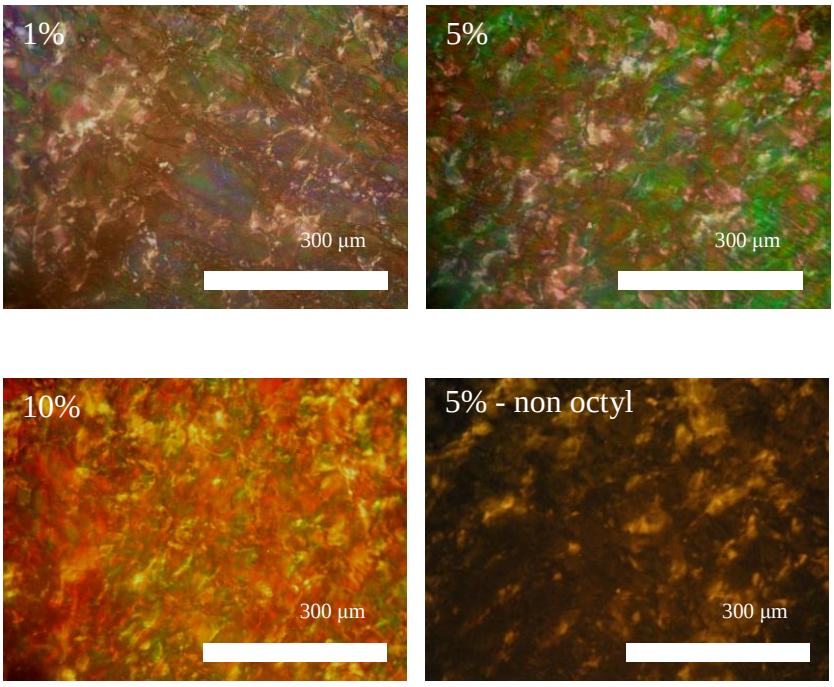

Figure 3-8. POM images of the films loaded with azobenzene doped 8CB.

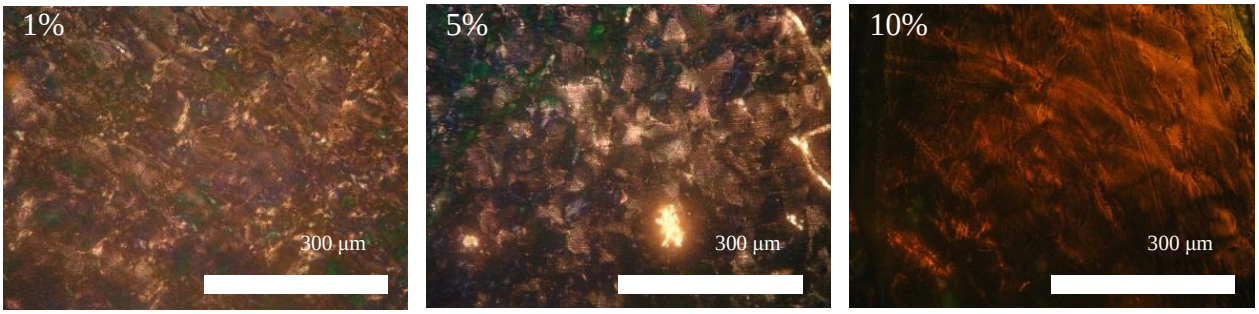

Figure 3-9. POM images of the composite films after irradiation with 365 nm light for 2 min.

The irradiated films were left out for 24 hours following their exposure to 365 nm light to allow for thermal and visible light assisted relaxation back to the trans configuration. POM images of these films reveal that their original state is restored (Figure 3-10). This process is reversible, and upon further irradiation and time should continue to cycle the LC between phases.

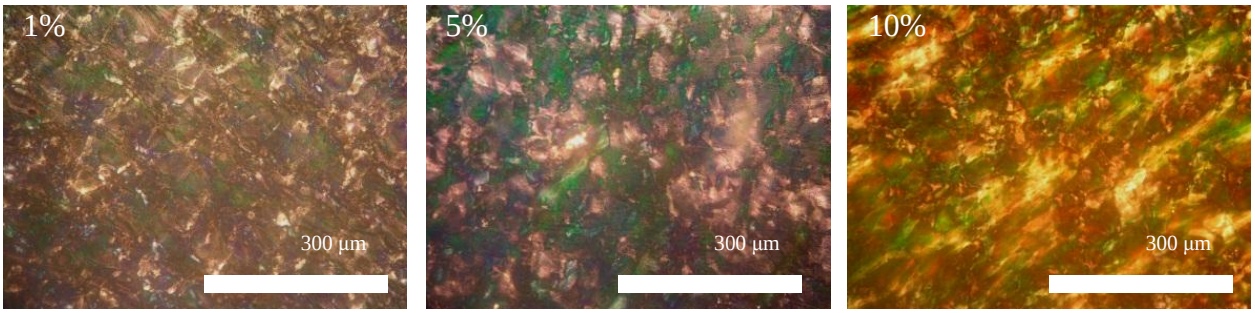

Figure 3-10. POM images of the irradiated films after exposure to visible light for 24 h.

The behaviour before, during, and after irradiation was also studied by UV-vis spectroscopy. Spectra were recorded for 8CB/ABD-1%@CNMO-octyl, 8CB/ABD-5%@CNMO-octyl, and 8CB/ABD-10%@CNMO-octyl before exposure to 365 nm light and then at subsequent intervals of 30 second exposures (Figure 3-11). The spectra shown display up to a total of 1.5 minutes exposure for 8CB/ABD-1%@CNMO-octyl and 2 minutes exposure time

for 8CB/ABD-5%@CNMO-octyl and 8CB/ABD-10%@CNMO-octyl at which point subsequent spectra taken showed no further changes. In all cases, it can be noted that isomerization from the trans to cis form occurs: the absorbance at ~350 nm corresponding to the π-π* transition decreases and the absorbance at ~450 nm corresponding to the n-π* transition increases after irradiation.

This behaviour is promising as it shows that doped LC can be used to switch the reflection in the films, but the strong orange colouration of the ABD and thus the loaded films limits potential applications.

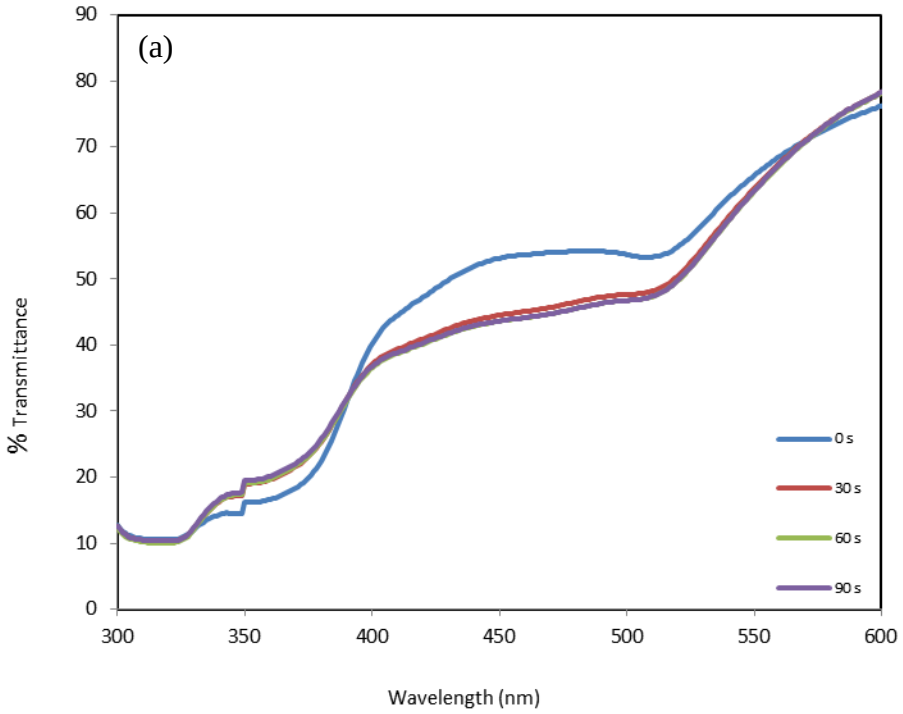

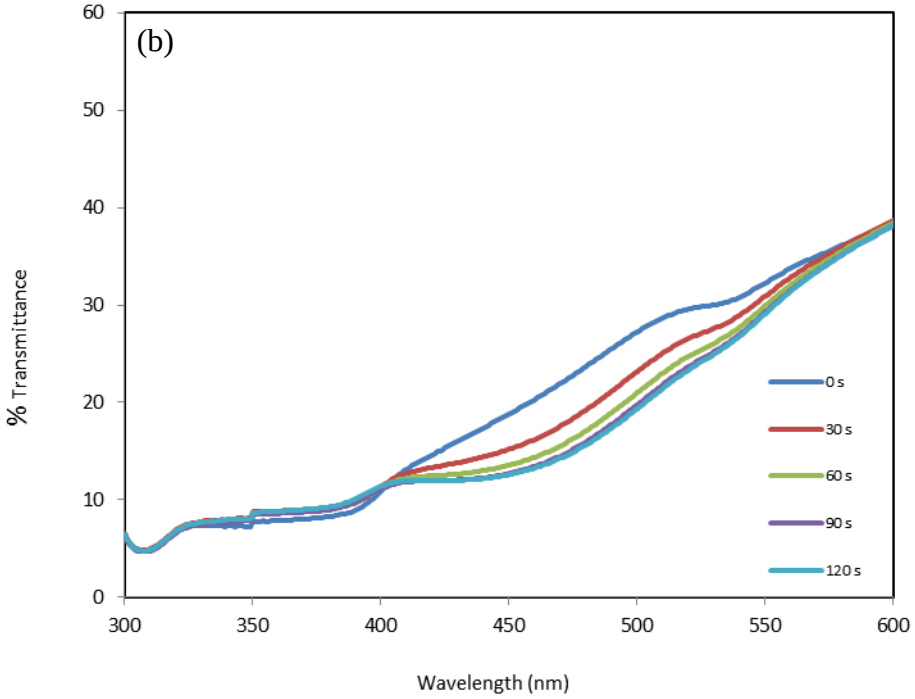

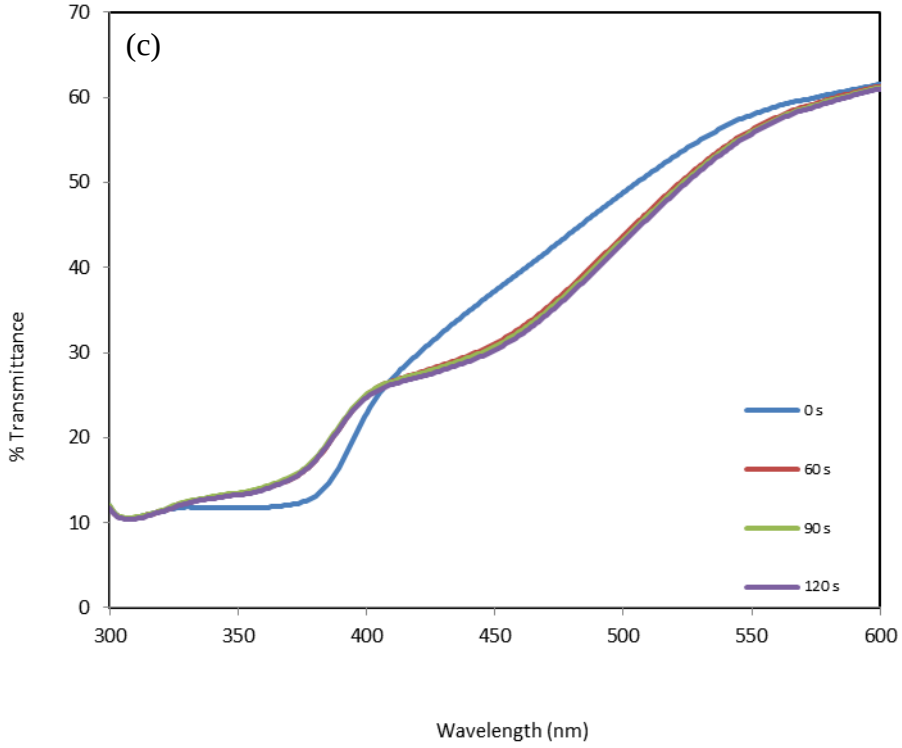

Figure 3-11. UV-vis spectra of the (a) 1% (b) 5% and (c) 10% dopant loaded films after various timed intervals of exposure to 365 nm light.

3.4 Conclusions

Diazene, 1-(4-butylphenyl)-2-(4-methoxyphenyl), an azobenzene derivative suitable for doping 8CB liquid crystal was synthesized and characterized. The molecule in its trans form stabilizes the liquid crystalline phase of 8CB, however, once irradiated at 365 nm and if present in high enough quantities, the bent cis form destabilizes the liquid crystal phase enough to cause a transition to isotropic. The photoisomerization switching behaviour within octyl functionalized chiral nematic organosilica films was fully studied by POM and UV-vis experiments. This approach should be expandable to other liquid crystals doped with azobenzene derivatives, allowing for the photoisomerization response of the CNMO to be readily tuned. The use of stimulus-induced switching of a guest to modify the optical properties of a mesoporous host may have possible applications in the development of dynamically switchable devices in displays or sensors.

Chapter 4: Conclusions and Future Work

4.1 Conclusions

Although mesoporous silicas and organosilicas have been synthesized through a template directed approach since 1992,[34,35,36,37,38] it is only over the past few years that nanocrystalline cellulose has been used to impart chiral nematic ordering on the resultant films.[40,41] These films display novel optical properties since the chiral nematic photonic structure is retained in the pores once the template is removed. There are many ways to tune their properties before drying to obtain films of different colours spanning the entire visible spectrum, however once these films are set their properties are essentially locked in. It has been shown that infiltration of the pores with isotropic liquids can shut off or dramatically reduce reflection due to the match or near match in refractive indexes, which is reversible upon removal.[40] The aim of this thesis has been to explore additional methods, specifically the use of various stimulus responsive guests, to reversibly modify the reflection in free-standing chiral nematic mesoporous silica and organosilica films after infiltration.

I have shown two different methods to modify the reflection in free-standing chiral nematic mesoporous silica and organosilica films. In Chapter 2, I selected two well known thermotropic liquid crystals, 5CB and 8CB, for infiltration and subsequent thermal cycling. Although infiltration resulted in an expected optical change due to the refractive index change, thermal cycling resulted in broad, incomplete transitions. Consequently I sought to modify the

pore walls to make them more slippery, and accomplished this through both octyl and phenyl functionalization. The modified pores allowed for more favorable orientation of the guest liquid crystal and resulted in sharp and complete transitions accompanied by dramatic optical changes. 8CB within octyl functionalized silica was identified to have the sharpest transition, so on transitioning to organosilica films I further explored this system, including with variable temperature UV-vis and POM experiments.

In Chapter 3, the addition of an azobenzene guest to the 8CB allowed similar behaviour to come about through irradiation of the composite films. Mixtures of 1, 5, and 10 % azobenzene dopant in 8CB were prepared and loaded into octyl functionalized organosilica films. The dopant molecule in its trans form stabilizes the liquid crystalline phase of 8CB, however, once irradiated at 365 nm and if present in high enough quantities, the bent cis form destabilizes the liquid crystal phase enough to cause a transition to isotropic, and results in an overall optical change of the composite film. This transition was shown to be reversible when left out in visible light or when allowed to relax thermally.

The work presented in this thesis presents significant findings on modifying the reflection in free-standing chiral nematic mesoporous silica and organosilica films by infiltration with stimulus responsive guests. I have shown optical changes brought about by two different stimuli, heat and light. These systems are very promising for applications such as in sensing and displays.

4.2 Future Work

While the results presented in this thesis are very promising, there is much left that can still be done. Expanding on the work in Chapter 2, it would be interesting to explore further triggers in addition to temperature that could be used to cycle 8CB within the octyl functionalized organosilica films. This system could also be expanded to include other LC guests in order to tune the temperature of the transition and thus the temperature at which the reflection of the films is altered. Solid-state NMR or additional studies to elucidate the exact orientation of the liquid crystal guest within the pores would also be something to pursue.

In Chapter 3, a potential drawback of the liquid crystal dopant system was the strong colouration of the ABD. It could be interesting to examine other photoswitchable molecules that absorb elsewhere in the spectrum to not only remove the colouration, but also tune the wavelength of irradiation needed for the isomerization and conformational change. Work is also underway to directly functionalize the walls of the organosilica with an azobenzene derivative moiety. In that case, the LC could be loaded into the functionalized films without a dopant, but the desired phase transition could in theory still be achieved through irradiation of the material with the appropriate wavelength of light.

References

[1] Zollinger, H., *Color Chemistry: Syntheses, Properties, and Applications of Organic Dyes and Pigments*, 3rd ed., Wiley-VCH, Veinheim, **2004**.

[2] Bandara, H. M. D.; Burdette, S. C. *Chem. Soc. Rev.* **2012**, *41*, 1809.

[3] Vignolini, S.; Rudall, P. J.; Rowland, A. V.; Reed, A.; Moyroud, E.; Faden, R. B.; Baumberg, J. J.; Glover, B. J.; Steiner, U. *PNAS* **2012**, *109*, 15712.

[4] Parker, A. R. *J. Opt. A: Pure Appl. Opt.* **2000**, *2*, R15.

[5] Kim, H.; Ge, J.; Kim, J.; Choi, S.-E.; Lee, H.; Lee, H.; Park, W.; Yin, Y.; Kwon, S. *Nature Photonics* **2009**, *3*, 534.

[6] Sharma, V.; Crne, M.; Park, J. O.; Srinivasarao, M. *Science* **2009**, *325*, 449.

[7] Tamaoki, N. *Adv. Mater.* **2001**, *13*, 1135.

[8] Bragg, W. L. *Proc. Cambridge Philos. Soc.* **1912**, *17*, 43.

[9] Joannopoulos, J. D.; Villeneuve, P. R.; Fan, S. *Nature* **1997**, *386*, 143.

[10] Johnson, S. G.; Joannopoulos, J. D., *Introduction to Photonic Crystals*, **2003**.

[11] Haibin, N.; Ming, W.; Wei, C. *Optics Express* **2011**, *19*, 25900.

[12] Schroden, R. C.; Al-Daous, M.; Blanford, C. F.; Stein, A. *Chem. Mater.* **2002**, *14*, 3305.

[13] Kubo, S.; Gu, Z.-Z.; Takahashi, K.; Fujishima, A.; Segawa, H.; Sato, O. *J. Am. Chem. Soc.* **2004**, *126*, 8314.

[14] Chandrasekhar, S., *Liquid Crystals*, 2nd ed., Cambridge University Press, Cambridge, **2002**.

[15] Reinitzer, F. *Monatsh. Chem.* **1888**, *9*, 421.

[16] De Vries, H. L. *Acta Cryst.* **1951**, *4*, 219.

[17] French, A. D.; Bertoniere, N. R.; Brown, R. M.; Chanzy, H.; Gray, D.; Hattori, K.; Glasser, W., in *Kirk-Othmer Encyclopedia of Chemical Technology*, 5th ed. (Ed.: Seidel, A.), John Wiley & Sons, New York, **2004**.

[18] Tashiro, K.; Kobayashi, M. *Polymer* **1991**, *32*, 1516.

[19] Habibi, Y.; Lucia, L. A.; Rojas, O. J.; *Chem. Rev.* **2010**, *110*, 3479.

[20] Sturcova, A.; His, I.; Apperley, D. C.; Sugiyama, J.; Jarvis, M. C. *Biomacromolecules* **2004**, *5*, 1333.

[21] Rånby, B. G. *Acta Chem. Scand.* **1949**, *3*, 649.

[22] Rånby, B. G.; Ribi, E. *Cell. Mol. Life Sci.* **1950**, *6*, 12.

[23] Revol, J.-F.; Bradford, H.; Giasson, J.; Marchessault, R. H.; Gray, D. G. *Int. J. Biol. Macromol.* **1992**, *14*, 170.

[24] Dong, X. M.; Kimura, T.; Revol, J.-F.; Gray, D. G. *Langmuir* **1996**, *12*, 2076.

[25] Dong, X. M.; Gray, D. G. *Langmuir* **1997**, *13*, 2404.

[26] Araki, J.; Wada, M.; Kuga, S.; Okano, T. *Langmuir* **2000**, *16*, 2413.

[27] Elazzouzi-Hafraoui, S.; Putaux, J.-L.; Heux, L. *J. Phys. Chem. B* **2009**, *113*, 11069.

[28] Sugiyama, J.; Chanzy, H.; Maret, G. *Macromolecules* **1992**, *25*, 4232.

[29] Lam, E.; Male, K. B.; Chong, J. H.; Leung, A. C. W.; Luong, J. H. T.; *Trends in Biotechnology* **2012**, *30*, 283.

[30] Kovacs, T.; Naish, V.; O'Connor, B.; Blaise, C.; Gagné, F.; Hall, L.; Trudeau, V.; Martel, P. *Nanotoxicology* **2010**, *4*, 255.

[31] Favier, V.; Chanzy, H.; Cavaille, J. Y. *Macromolecules* **1995**, *28*, 6365.

[32] Mann, S.; Ozin, G. A. *Nature* **1996**, *382*, 313.

[33] Sing, K. S. W.; Everett, D. H.; Haul, R. A. W.; Moscou, L.; Pierotti, R. A.; Rouquerol, J.; Siemieniewska, T. *Pure Appl. Chem.* **1985**, *57*, 603.

[34] Kresge, C. T.; Leonowicz, M. E.; Roth, W. J.; Vartuli, J. C.; Beck, J. S. *Nature* **1992**, *359*, 710.

[35] Beck, J. S.; Vartuli, J. C.; Roth, W. J.; Leonowicz, M. E.; Kresge, C. T.; Schmitt, K. D.; Chu, C. T. W.; Olson, D. H.; Sheppard, E. W.; McCullen, S. B.; Higgins, J. B.; Schlenker, J. L. *J. Am. Chem. Soc.* **1992**, *114*, 10834.

[36] Inagaki, S.; Guan, S.; Fukushima, Y.; Ohsuna, T.; Terasaki, O. *J. Am. Chem. Soc.* **1999**, *121*, 9611.

[37] Asefa, T.; MacLachlan, M. J.; Coombs, N.; Ozin, G. A. *Nature* **1999**, *402*, 867.

[38] Melde, B. J.; Holland, B. T.; Blanford, C. F.; Stein, A. *Chem. Mater.* **1999**, *11*, 3302.

[39] Dujardin, E.; Blaseby, M.; Mann, S. *J. Mater. Chem.* **2003**, *13*, 696.

[40] Shopsowitz, K. E.; Qi, H.; Hamad, W. Y.; MacLachlan, M. J. *Nature* **2010**, *468*, 422.

[41] Shopsowitz, K. E.; Hamad, W. Y.; MacLachlan, M. J. *J. Am. Chem. Soc.* **2012**, *134*, 867.

[42] Collins, P., *Liquid Crystals*, Princeton University Press, Princeton and Oxford, **2002**.

[43] Heilmeier, G. H.; Helfrich, W. *Appl. Phys. Lett.* **1970**, *16*, 155.

[44] Heilmeier, G. H. *Scientific American* **1970**, *222*, 100.

[45] Fergason, J. L. *Optical Spectra* **1978**, *12*, 54.

[46] Williams, R. *Nature* **1963**, *199*, 273.

[47] Fergason, J. L.; Goldberg, N. N.; Nadalin, R. J. *Mol. Cryst.* **1966**, *1*, 309.

[48] Pan, J.; Hamad, W.; Straus, S. K. *Macromolecules* **2010**, 43, 3851.

[49] Beck, S.; Bouchard, J.; Berry, R. *Biomacromolecules* **2011**, *12*, 167.

[50] Dong, X. M.; Revol, J.-F.; Gray, D. G. *Cellulose* **1998**, *5*, 19.

[51] Fergason, J. L. *Mol. Cryst. Liq. Cryst.* **1966**, *1*, 293.

[52] Saeva, F. D. *Mol. Cryst. Liq. Cryst.* **1972**, *18*, 375.

[53] Sackmann, E.; Voss, J. *Chem. Phys. Lett.* **1972**, *14*, 528.

[54] Sackmann, E.; Möhwald, H. *J. Chem. Phys.* **1973**, *58*, 5407.

[55] Fergason, J. L.; Taylor, T. R.; Harsch, T. B. *Electro-Technology* **1970**, *85*, 41.

[56] Arsenault, A. C.; Puzzo, D. P.; Manners, I.; Ozin, G. A. *Nature Photonics* **2007**, *1*, 468.

[57] Aguirre, C. I.; Reguera, E.; Stein, A. *Adv. Func. Mater.* **2010**, *20*, 2565.

[58] Arsenault, A. C.; Clark, T. J.; von Freymann, G.; Cademartiri, L.; Sapienza, R.; Bertolotti, J.; Vekris, E.; Wong, S.; Kitaev, V.; Manners, I.; Wang, R. Z.; John, S.; Wiersma, D.; Ozin, G. A. *Nature Materials* **2006**, *5*, 179.

[59] Kitzerow, H.-S.; Lorenz, A.; Matthias, H., in *Nanophotonic Materials*, (Eds.: Wehrspohn, R. B.; Kitzerow, H.-S.; Busch, K.), Wiley-VCH, Weinheim, **2008**.

[60] Kitzerow, H.-S.; Lorenz, A.; Matthias, H. *Phys. Stat. Sol. (a)* **2007**, *204*, 3754.

[61] Mertens, G.; Röder, T.; Matthias, H.; Marsmann, H.; Kitzerow, H.-S. R.; Schweizer, S. L.; Jamois, C.; Wehrspohn, R. B.; Neubert, M. *Appl. Phys. Lett.* **2003**, *83*, 3036.

[62] Martz, J.; Ferrini, R.; Nüesch, F.; Zuppiroli, L.; Wild, B.; Dunbar, L. A.; Houdré, R.; Mulot, M.; Anand, S. *J. Appl. Phys.* **2006**, *99*, 103105.

[63] Mertens, G.; Wehrspohn, R. B.; Kitzerow, H.-S.; Matthias, S.; Jamois, C.; Gösele, U. *Appl. Phys. Lett.* **2005**, *87*, 241108.

[64] Ghattan, Z.; Hasek, T.; Wilk, R.; Shahabadi, M.; Koch, M. *Optics Commun.* **2008**, *281*, 4623.

[65] Kubo, S.; Gu, Z.-Z.; Takahashi, K.; Fujishima, A.; Segawa, H.; Sato, O. *J. Am. Chem. Soc.* **2004**, *126*, 8314.

[66] Robbie, K.; Brett, M. J. *J. Vac. Sci. Technol. A* **1997**, *15*, 1460.

[67] Robbie, K.; Brett, M. J.; Lakhtakia, A. *J. Vac. Sci. Technol. A* **1995**, *13*, 2991.

[68] Robbie, K.; Brett, M. J.; Lakhtakia, A. *Nature* **1996**, *384*, 616.

[69] Kennedy, S. R.; Sit, J. C.; Broer, D. J.; Brett, M. J. *Liquid Crystals* **2001**, *28*, 1799.

[70] Hodgkinson, I.; Wu, Q. H. *Adv. Mater.* **2001**, *13*, 889.

[71] Robbie, K.; Broer, D. J.; Brett, M. J. *Nature* **1999**, *399*, 764.

[72] Sit, J. C.; Broer, D. J.; Brett, M. J. *Liquid Crystals* **2000**, *27*, 387.

[73] Wakefield, N. G.; Elias, A. L.; Brett, M. J.; Sit, J. C.; Broer, D. J. *Mol. Cryst. Liq. Cryst.* **2007**, *475*, 85.

[74] Sit, J. C.; Kennedy, S. R.; Broer, D. J.; Brett, M. J. *Liquid Crystals IV Proc. SPIE* **2000**, *4107*, 133.

[75] Sit, J. C.; Broer, D. J.; Brett, M. J. *Adv. Mater.* **2000**, *12*, 371.

[76] Shopsowitz, K. E.; Hamad, W. Y.; MacLachlan, M. J. *Angew. Int. Chem. Ed.* **2011**, *50*, 10991.

[77] Revol, J.-F.; Bradford, H.; Giasson, J.; Marchessault, R. H.; Gray, D. G. *Int. J. Biol. Macromol.* **1992**, *14*, 170.

[78] Hamad, W. Y. *ACS Symposium Series* **2011**, *1067*, 301.

[79] Hamad, W. Y. *Can. J. Chem. Eng.* **2006**, *84*, 513.

[80] Klemm, D.; Kramer, F.; Moritz, S.; Lindstroem, T.; Ankerfors, M.; Gray, D.; Dorris, A. *Angew. Int. Chem. Ed.* **2011**, *50*, 5438.

[81] Krast, P. P.; Madshusudana, N. V. *Mol. Cryst. Liq. Cryst.* **1976**, *36*, 51.

[82] Gnatyuk, I. I.; Puchkovskaya, G. A.; Goltsov, Yu. G.; Matkovskaya, L. A.; Drozd, M. *J. Therm. Anal. Calorim.* **2000**, *62*, 365.

[83] Kralj, S.; Zidansek, A.; Lahajnar, G.; Zumer, S.; Blinc, R. *Phys. Rev. E* **2000**, *62*, 718.

[84] Iannacchione, G. S.; Crawford, G. P.; Qian, S.; Doane, J. W.; Finotello, D.; Zumer, S. *Phys. Rev. E* **1996**, *53*, 2402.

[85] Frunza, L.; Kosslick, H.; Fricke, R. *H.-G. Sys. Nano. Cryst.* **2003**, 84.

[86] Horn, R. G. *J. Phys. France* **1978**, *39*, 105.

[87] Han, Y.; Pacheco, K.; Bastiaansen, C. W. M.; Broer, D. J.; Sijbesma, R. P. *J. Am. Chem. Soc.* **2010**, *132*, 2961.

[88] Wittebrood, M. M.; Luijendijk, D. H.; Stallinga, S.; Rasing, T.; Musevic I. I. *Phys. Rev. E.* **1996**, *54*, 5232.

[89] Iannacchione, G. S.; Finotello, D. *Phys. Rev. Lett.* **1992**, *69*, 2094.

[90] Iannacchione, G. S.; Crawford, G. P.; Zumer, S.; Doane, J. W.; Finotello, D. *Phys. Rev. Lett.* **1993**, *71*, 2595.

[91] Mitscherlich, E. *Ann. Pharm.* **1834**, *12*, 311.

[92] Hunger, K., *Industrial Dyes: Chemistry, Properties and Applications*, Wiley-VCH, Weinheim, **2003**.

[93] Hartley, G. S. *Nature* **1937**, *140*, 281.

[94] Rau, H.; Lueddecke, E. *J. Am. Chem. Soc.* **1982**, *104*, 1616.

[95] Zimmerman, G.; Chow, L.-Y.; Paik, U.-J. *J. Am. Chem. Soc.* **1958**, *80*, 3528.

[96] Natansohn, A.; Rochon, P. *Chem. Rev.* **2002**, *102*, 4139.

[97] Cojocariu, C.; Rochon, P. *Pure Appl. Chem.* **2004**, *76*, 1479.

[98] Legge, C. H.; Mitchell, G. R. *J. Phys. D: Appl. Phys.* **1992**, *25*, 492.

[99] Kurihara, S.; Nomiyama, S.; Nonaka, T. *Chem. Mater.* **2000**, *12*, 9.

[100] Junge, D. M.; McGrath, D. V. *J. Am. Chem. Soc.* **1999**, *121*, 4912.